

PL-TR-97-2108

**CHARACTERIZATION OF UV EMISSIONS
RESULTING FROM ELECTRONIC ENERGY
TRANSFER IN ATMOSPHERIC MOLECULES**

**Anthony V. Dentamaro
Joseph M. Thomas**

**ORION International Technologies, Inc.
2201 Buena Vista Dr. SE, Suite 211
Albuquerque, NM 87106**

November 1997

**Final Report
November 1992 - March 1997**

Approved for Public Release; Distribution Unlimited



**PHILLIPS LABORATORY
Directorate of Geophysics
AIR FORCE MATERIEL COMMAND
HANSCOM AFB, MA 01731-3010**

19980113 013

DTIC QUALITY INSPECTED 3

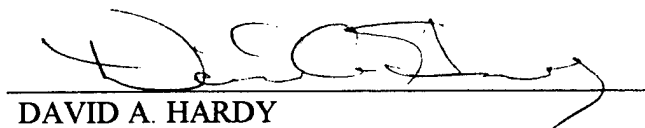
"This technical report has been reviewed and is approved for publication"



ROBERT A. MORRIS
Contract Manager



ROBERT A. MORRIS
Branch Chief



DAVID A. HARDY
Division Director

This report has been reviewed by the ESC Public Affairs Office (PA) and is releasable to the National Technical Information Service (NTIS).

Qualified requestors may obtain additional copies from the Defense Technical Information Center (DTIC). All others should apply to the National Technical Information Service (NTIS).

If your address has changed, if you wish to be removed from the mailing list, if the addressee is no longer employed by your organization, please notify PL/IM, 29 Randolph Road, Hanscom AFB, MA 01731-3010. This will assist us in maintaining a current mailing list.

Do not return copies of this report unless contractual obligations or notices on a specific document require that it be returned.

REPORT DOCUMENTATION PAGE

Form Approved
OMB No. 0704-0188

Public reporting burden for this collection of information to average 1 hour per response, including the time for reviewing instructions, searching existing data sources, gathering and maintaining the data needed, and completing and reviewing the collection of information. Send comments regarding this burden estimate or any other aspect of this collection of information, including suggestions for reducing this burden, to Washington Headquarters Services, Directorate for Information Operations and Reports, 1215 Jefferson Davis Highway, Suite 1204, Arlington, VA 22202-4302, and to the Office of Management and Budget, Paperwork Reduction Project (0704-0188), Washington, DC 20503.

1. AGENCY USE ONLY (Leave blank)	2. REPORT DATE November 97	3. REPORT TYPE AND DATES COVERED Final Report (November 1992 - March 1997)
----------------------------------	-------------------------------	---

4. TITLE AND SUBTITLE Characterization of UV Emissions Resulting From Electronic Energy Transfer In Atmospheric Molecules	5. FUNDING NUMBERS PE 61102F PR 2303 TA GJ WU AA Contract F19628-92-C-0161
--	---

6. AUTHOR(S) Anthony V. Dentamaro Joseph M. Thomas	
--	--

7. PERFORMING ORGANIZATION NAME(S) AND ADDRESS(ES) ORION International Technologies, Inc 6501 Americas Parkway, NE, Suite 200 Albuquerque, NM 87110	8. PERFORMING ORGANIZATION REPORT NUMBER TR97-003
--	--

9. SPONSORING/MONITORING AGENCY NAME(S) AND ADDRESS(ES) Phillips Laboratory 29 Randolph Road Hanscom AFB, MA 01731-3010 Contract Manager: Robert Morris/GPID	10. SPONSORING/MONITORING AGENCY REPORT NUMBER PL-TR-97-2108
--	---

11. SUPPLEMENTARY NOTES

12a. DISTRIBUTION/AVAILABILITY STATEMENT APPROVED FOR PUBLIC RELEASE; DISTRIBUTION UNLIMITED	12b. DISTRIBUTION CODE
---	------------------------

13. ABSTRACT (Maximum 200 words)

State-specific experiments were performed which studied collision induced electronic transitions (CIET) in a diatomic molecule. These optical-optical double resonance (OODR) experiments employed a resonance enhanced multiphoton ionization (REMPI) technique for purposes of detection. A strong dependence on Franck-Condon factor (FCF) and small energy gap, as well as a propensity for conservation of rotational angular momentum have become trademarks of our CIET experiments. Present theoretical models of these processes are not able to fully reproduce the observed results, thus making it important to perform experiments which consider a wide range of energy gaps and FCF. The volume of our data has led to the development of an empirical branching ratio model which appears to be quite accurate and useful in predicting deactivation rate constants for CIET in various diatomic molecules. These results have been incorporated into a model of atmospheric Lyman-Birge-Hopfield (LBH) emissions.

We report branching fraction measurements for the energy transfer reactions $N_2(A \ 3\Sigma_u^+, v') + NO(X \ 2\Pi_r, v''=0) \rightarrow N_2(X \ 1\Sigma_g^+, v'') + NO(A \ 2\Sigma^+, v' \leq 1) + NO(B \ 2\Pi_r, v''=0)$ and $CO(a \ 3\Pi, v' \leq 3) + NO(X \ 2\Pi_r, v''=0) \rightarrow CO(X \ 1\Sigma^+, v'') + NO(A \ 2\Sigma^+, v' \leq 2) + NO(B \ 2\Pi_r, v''=0)$. In addition we discuss the $N(4S) + NO(X \ 2\Pi_r)$ product channel measured in the reaction $N_2(A \ 3\Sigma_u^+, v') + O(3P)$.

14. SUBJECT TERMS. Collision induced electronic transistors Diatomic molecules Metastable molecular nitrogen Optical-optical double resonance (OODR) Atmospheric models Branching functions Resonance enhanced multiphoton ionization (REMPI) Energy transfer reactions Franck-Condon factor (FCF)	Active nitrogen bimolecular energy transfer branching fractions carbon monoxide $CO(a \ 3\Pi)$ emission spectra energy transfer kinetics Metastable nitrogen $N_2(A \ 3\Sigma_u^+)$	nitric oxidenitrogen monoxide $NO(A \ 2\Sigma^+)$ $NO(B \ 2\Pi_r)$ photoelectric emission spectroscopy plasma chemistry product emissions rapidly pumped discharge-flow reactor rotational temperature synthetic spectra vibrational temperature	15. NUMBER OF PAGES 60
			16. PRICE CODE

17. SECURITY CLASSIFICATION OF REPORT UNCLASSIFIED	18. SECURITY CLASSIFICATION OF THIS PAGE UNCLASSIFIED	19. SECURITY CLASSIFICATION OF ABSTRACT UNCLASSIFIED	20. LIMITATION OF ABSTRACT SAR
---	--	---	-----------------------------------

(This page intentionally left blank)

TABLE OF CONTENTS

<u>SECTION</u>	<u>PAGE</u>
STUDY OF THE COLLISION INDUCED ELECTRONIC TRANSITIONS	1
1 INTRODUCTION	1
2 EXPERIMENTAL	3
3 CIET RESULTS AND MODELS	3
4 APPLICATIONS	5
5 DISCUSSION	6
6 REFERENCES	8
7 PUBLICATIONS	9
8 MEETINGS	9
 CHARACTERIZATION OF UV EMISSIONS RESULTING FROM ELECTRONIC ENERGY TRANSFER IN ATMOSPHERIC MOLECULES	11
1 INTRODUCTION	11
2 EXPERIMENTAL	18
3 RESULTS AND DISCUSSION.	25
3.1 BRANCHING FRACTIONS OF THE PRODUCT AND EMISSIONS OBSERVED AS A FUNCTION OF v' IN THE ENERGY TRANSFER REACTION	25
3.2 BRANCHING FRACTIONS OF THE PRODUCT NO(A $2\Sigma^+, v'=0, 1$ AND 2) AND NO(B $2\Pi_r, v'=0$) EMISSIONS OBSERVED AS A FUNCTION OF v' IN THE ENERGY TRANSFER REACTION CO(a $3\Pi, v'$) + NO(X $2\Pi_r, v''=0$)	31
3.2.1 Analysis of the NO(A $2\Sigma^+, v'$) and NO(B $2\Pi_r, v'$) Emissions.	31
3.2.2 Comparison between the N ₂ (A $3\Sigma_u^+$) and CO(a 3Π)	37
3.3 AN UPPER LIMIT ON THE FORMATION OF NO(X $2\Pi_r$) IN THE REACTIONS N ₂ (A 3) + O(3P) AND N ₂ (A 3) + O ₂ (X 3) AT 298 K.	38
3.4 PROGRAM ENHANCEMENTS TO THE NO(A $2\Sigma^+, v'$ X $2\Pi_r, v''$) γ BANDS SYNTHETIC SPECTRUM GENERATION CODE	43
3.5 GENERAL MODIFICATIONS AND CODE ENHANCEMENTS	48
4 CONCLUSIONS	48
5 REFERENCES	51
6 PRESENTATIONS	55
7 PUBLICATIONS	55
8 KEYWORD LISTING	56

STUDY OF THE COLLISION INDUCED ELECTRONIC TRANSITIONS $a^1\Pi_g(v') \rightarrow w^1\Delta_u(v'')$ in N_2

Abstract

State-specific experiments were performed which studied collision induced electronic transitions (CIET) in a diatomic molecule. These optical-optical double resonance (OODR) experiments employed a resonance enhanced multiphoton ionization (REMPI) technique for purposes of detection. A strong dependence on Franck-Condon factor (FCF) and small energy gap, as well as a propensity for conservation of rotational angular momentum have become trademarks of our CIET experiments. Present theoretical models of these processes are not able to fully reproduce the observed results, thus making it important to perform experiments which consider a wide range of energy gaps and FCF. The volume of our data has led to the development of an empirical branching ratio model which appears to be quite accurate and useful in predicting deactivation rate constants for CIET in various diatomic molecules. These results have been incorporated into a model of atmospheric Lyman-Birge-Hopfield (LBH) emissions.

1 INTRODUCTION

This report discusses the latest results in our study of collision-induced electronic transitions (CIET) in N_2 . The first $a^1\Pi_g(v') \rightarrow w^1\Delta_u(v'')$ transition in N_2 had only recently been observed in our last report, and the importance of this to our modelling of atmospheric emissions was discussed. We believe to have recently seen a second $a \rightarrow w$ transition with surprisingly different results from the first. We discuss this observation in the light of previous measurements.

State-specific experiments which study CIET in a diatomic molecule have been undertaken for over a decade. As has been stated many times, these experiments show a collisional propensity for conserving the total angular momentum, J , for CIET, thereby allowing for the accurate determination of the energy gaps traversed in CIET. Present theoretical models of these processes still fall well short of successfully describing the large transfer of electronic to translational energy which is observed. Quantum scattering calculations by Alexander, Werner

and co-workers^{1,2} have predicted the correct general propensities and cross-sections for the small energy gaps, but there is a large disagreement of a few orders of magnitude for the large energy gap transitions. Experiments³⁻⁶ using the same technique of optical-optical double resonance (OODR) on the isoelectronic molecules CN, N₂⁺ and CO⁺ have had interesting results. These experiments not only show a propensity for small ΔJ , but also for a strong correlation with the Franck-Condon factor (FCF).

We have studied the Lyman-Birge-Hopfield (LBH) bands of nitrogen (N₂; a¹Π_g-X¹Σ_g⁺) and collisional quenching between the lowest-lying singlet states of molecular nitrogen via two photon⁷ and resonance enhanced multiphoton ionization (REMPI) techniques⁸⁻¹¹ for several years now. As in the experiments involving N₂⁺ described previously, there are no perturbations in the collisionally-coupled a¹Π_g and a¹Σ_u⁻ states of the isolated N₂ molecule. We previously reported^{10,11} on the first direct double resonance observation of CIET from the a(v=0) level to the a'(v=0 and 1) levels using REMPI spectroscopy. The a'(v=1) level, omitted in other room-temperature collisional models, was seen to participate in the CIET process in spite of being 295 cm⁻¹ endothermic with respect to the a(v=0) level. The inclusion of the a'(v=1) level yields a more accurate collisional deactivation model as well as state-specific quenching rates. The process of collisional deactivation for N₂ and N₂⁺ are strikingly similar despite the lack of ion-induced dipole for the neutral case. Although the cross-sections for collisional quenching is almost an order of magnitude less for N₂ compared to N₂⁺ as expected, the CIET propensities are similar. In addition, the cross-sections increase when the temperature is decreased for both cases indicating the attractive part of the interaction potential is important.

In addition to the initial observation of a(v=0) → a''(v=0,1) CIET, we also have reported on the observation of a(v=1) → a'(v=1,2) and the branching ratios and collisional deactivation rates have been determined for these transitions. Our work was then systematically extended to the a(v=2) level, and possible transitions to the a'(v=2,3) levels were studied. We also looked for and found evidence of the a¹Π_g(v=2) → w¹Δ_u(v=0) CIET and found it to be surprisingly strong.

Equally surprising then was our inability to see the $a(v=3) \rightarrow w(v=1)$ transition which should have been even more efficient than $a(v=2) \rightarrow w(v=0)$. Finally, we were able to observe the $a(v=4) \rightarrow w(v=2)$ CIET, which was seen to be weak.

2 EXPERIMENTAL

The setup for our laboratory experiments which examine CIET in various species has been described many times. Optical-optical double resonance (OODR) experiments involve the use of a "pump" laser to prepare the molecule into a specific excited state and a "probe" laser to examine states to which collision induced energy is transferred. For these particular experiments, we examine the CIET process N_2 $a(v=2) \rightarrow a'(v=3)$ and $a(v=2) \rightarrow w(v=0)$. The "pump" laser is tuned to a specific line of the $a-X(2,0)$ band which selectively populates a single rotational level in the $a(v=2)$ manifold. Collisions with rare gas atoms (He, Ar, Kr) or N_2 molecules cause energy transfer to other rotational levels of the $a(v=2)$ level and also to the $a'(v=2,3)$ and $w(v=0)$ states. We did not look for rotational energy transfer within the $a(v=2)$ manifold, although this could have easily been done. Instead, we were much more interested in the electronic transitions for now. CIET is monitored by tuning the "probe" laser to the lines of the $y-a'(1,3)$ and $y-w(1,0)$ bands. Having the same up state for the probing of both transitions allows for a direct comparison of the two. The pump and probe laser pulses are time delayed by about four nanoseconds to insure that only single collision events are seen. Collision induced vibrational energy transfer within the same electronic state has not yet been seen in state specific experiments at these time scales.

3 CIET RESULTS AND MODELS

CIET experiments¹² have been performed recently for the case of collisional coupling between $a(v=2)$ and $a'(v=2,3)$ and $w(v=0)$ levels. We have reported in the past that the transition $a(v=2) \rightarrow a'(v=2)$ should be exceedingly difficult to observe since our empirical model (which is reviewed below) predicts that this transition should be roughly 350 times weaker than that for $a(v=2) \rightarrow a'(v=3)$. Indeed, we have looked for the $a(v=2) \rightarrow a'(v=2)$ transition many times in the past and have failed to observe it. The main reason for this large branching ratio is the fact

that the $a(v=2) \rightarrow a'(v=3)$ traverses only a 70 cm^{-1} energy gap and possesses a sizeable Franck-Condon factor ($q_{2,3}=0.185$). This means that this transition is very efficient.

It was therefore surprising to find that we were able to see the $a(v=2) \rightarrow w(v=0)$ transition. I believe that this is the first time that collisional coupling of the a and w states has been observed. This transition was studied on several occasions in this laboratory with no success and was thought to be unobservable. Both the $y^1\Pi_g - w^1\Delta_u(1,0)$ and $k^1\Pi_g - w^1\Delta_u(1,0)$ bands were observed as were the bands $y^1\Pi_g - a'^1\Sigma_u^-(1,3)$ and $k^1\Pi_g - a'^1\Sigma_u^-(1,3)$. This also marks our first observation of the mutually perturbed y and k states. The $a(v=2) \rightarrow w(v=0)$ transition traverses an energy gap of 557 cm^{-1} and has an FCF of $q_{2,0}=0.037$.

Making the observation of the $y - w(1,0)$ particularly difficult is the fact that discharging of the tantalum plates used in our collection procedure inadvertently introduced trace amounts of NO to our system. The NO A-X (0,0) "gamma" band starts at about 2269\AA and is shaded to the blue. The P branch bandhead for $y - w(1,0)$ is at 2264.13\AA and is also shaded to the blue, superimposing on the very intense lines of the NO gamma band. After careful examination of the data, the $y-w$ band was discovered, and spectra were taken at liquid nitrogen temperature ($T=78\text{K}$) in order to "freeze out" the NO background. Branching ratios were measured, and it was found that the transition to the $a'(v=3)$ state is only about five times stronger than that to the $w(v=0)$ state. This result is quite unexpected, but using this branching ratio allows us to fit the data for the radiative decay of the $a(v=2)$ state which were unreconcilable before these experiments were completed.

We quickly outline the basis of our empirical energy gap model one more time. Although determining a simple, comprehensive energy gap dependence from the data would be unrealistic, we have developed an empirical model which can predict the *branching ratio* for cases where

there are competing CIET's as a function of the smaller energy gap. Using primarily N_2^+ data, we find that

$$k_{ij}/k_{im} = (q_{ij}/q_{im}) R, \quad (1)$$

where

$$R = 14.8 + 0.043(\Delta E_{ij}), \quad (2)$$

where ΔE_{ij} is the smaller of the two energy gaps. It turns out, recently measured branching ratios for CIET in $^{15}N_2^+$ and N_2 have been seen to fit the predictions of the empirical model exceptionally well. In addition, this model proved instrumental in determining the branching ratio and rate constants for $CO^+ A(v=4) \rightarrow X(v=12,13)$ where the data was difficult to analyze.

4 APPLICATIONS

We have described how the results of the above-described experiments can be applied to supplement current models for the prediction of atmospheric LBH emissions which are observed in dayglow and aurorae. The primary processes which are expected to determine the vibrational distribution of emissions from the N_2 a state include the initial population of these states via electron impact excitation and radiative cascade between the vibrational levels of the a, a' and w singlet states. We add the effects of CIET to these processes.

We construct a general form for the $v' \rightarrow v''$ deactivation constants:

$$k = \alpha q_{v'v''} f(\Delta E) g(T), \quad (3)$$

where α is a species-dependent scaling factor, $q_{v'v''}$ is the FCF, $f(\Delta E)$ is the energy gap dependence and $g(T)$ is the temperature dependence.

The success of the empirical branching ratio model indicates that there may be some common type of energy dependence for all the available CIET data. By fitting this data to a common functional form, we were able to get an approximate expression for $f(\Delta E)$:

$$f(\Delta E) = (a|\Delta E| + 1)^{-1}, \quad (4)$$

where $a=0.064$ for $\Delta E > 0$ and 0.096 for $\Delta E < 0$, and ΔE is in cm^{-1} . This form fits the CIET data within each species and also reproduces the predictions of the branching ratio model.

The temperature dependence $g(T)$ was constructed such that the results of room temperature ($T=298\text{K}$) laboratory experiments could be extrapolated to the temperatures characteristic of the atmosphere at auroral altitudes. This dependence was derived from the collision complex model proposed by Lin, *et al.*¹³ and reflects the experimental observation that for CIET processes, the cross section increases with decreasing temperature. We get

$$g(T) = \xi \exp(\epsilon/kT), \quad (5)$$

where $\xi = \exp(-\epsilon/208)$, and ϵ is the intermolecular well depth in cm^{-1} for the attractive potential between colliders.

5 DISCUSSION

The observation of the N_2 $a(v=2) \rightarrow w(v=0)$ transition is a very important step in the refinement of our atmospheric LBH emissions model. In the past, the $a \leftrightarrow w$ transitions were treated the same as the $a \leftrightarrow a'$ transitions. The results of our experiments show the former family of transitions to be about five times stronger than previously thought. It should be mentioned that in calculating the branching ratio of transitions to the $a'(v=3)$ state versus that to the $w(v=0)$ state, the electric dipole moments of the two transitions were taken to be approximately equal, and the results of our fits have seemed to borne this out. In fact, increasing the importance of the $a \leftrightarrow w$ transitions in the atmospheric model does nothing to hurt our fit of the relative vibrational populations of the N_2 a state and may actually represent an improvement.

However, the news is not all good. Since the $a(v=2) \rightarrow w(v=0)$ transition is fairly easy to observe, it is expected that transitions involving the higher vibrational levels of these states should be even easier to see. This is because as we go up the vibrational ladder, the transitions [$a(v=3) \rightarrow w(v=1)$, $a(v=4) \rightarrow w(v=2)$, etc.] possess only slightly larger energy gaps but much stronger FCFs. As a matter of fact, these $a \rightarrow w$ FCFs are greater than those of the competing

$a \rightarrow a'$ transitions for $a(v > 2)$. However, all attempts to observe the $a(v=3) \rightarrow w(v=1)$ transition have been fruitless thus far. In addition to this, only recently do we feel we have succeeded in observing the $a(v=4) \rightarrow w(v=2)$ transition, but have found it to be exceedingly weaker than first expected. The FCF for this $a \rightarrow w$ transition is six times greater than the competing $a(v=4) \rightarrow a'(v=5)$ transition, and the energy gap is less than twice as big. This means that the CIET to the a' state should be inefficient, thus leaving the CIET to the w state as practically the only open channel. Although the $a(v=4) \rightarrow a'(v=5)$ transition has not yet been seen, probably due to its expectedly low rate constant, the CIET to the w state is itself very weak and difficult to identify.

We previously discussed a possible explanation of the surprising efficiency of the $a(v=2) \rightarrow w(v=0)$ CIET compared to the rest of the available data. The suggestion was that we are not really seeing a "clean" transition in the $a(v=2) \rightarrow w(v=0)$ data. Since the $a(v=2)$ and $a'(v=3)$ levels are nearly resonant, it is possible that at the pressures at which we are working, the two states could be equilibrating, thus leaving the transition to $w(v=0)$ the most favorable channel. For the higher vibrational manifolds of the singlet system, this resonant situation never really occurs again, thus making transitions to the w state that much more difficult to observe.

Experiments do continue on these systems. Any data that are collected are useful in that they contribute to the input of our atmospheric model. It appears at this time that the $a \rightarrow w$ transitions, and therefore the reverse $w \rightarrow a$ CIET are weaker than thought, and the models must be modified to reflect this difference. Quantitative results are not available at this time.

6 REFERENCES

- 1) H.-J. Werner, B. Follmeg, M.H. Alexander and D. LeMoine, "Quantum scattering studies of electronically inelastic collisions of CN ($X^2\Sigma^+$, $A^2\Pi$) with He," *J. Chem. Phys.* **91**, 5425 (1989).
- 2) A. Berning and H.-J. Werner, "Quantum scattering studies of electronically inelastic collisions of N_2^+ ($X^2\Sigma_g^+$, $A^2\Pi_u$) with He," *J. Chem. Phys.* **100**, 1953 (1994).
- 3) N. Furio, A. Ali and P.J. Dagdigian, "Collisionless and collision-induced B-X emission from laser-excited CN $A^2\Pi$ $v=10$ rotational levels," *Chem. Phys. Lett.* **125**, 561 (1986).
- 4) G. Jihua, A. Ali and P.J. Dagdigian, "State-to-state collisional interelectronic and intraelectronic energy transfer involving CN $A^2\Pi$ $v=3$ and $X^2\Sigma^+$ $v=7$ rotational levels," *J. Chem. Phys.* **85**, 7089 (1986).
- 5) A.V. Dentamaro and D.H. Katayama, "Collision induced transitions between $A^2\Pi_i$ ($v=0$) and $X^2\Sigma^+$ ($v=10$) states of CO^+ ," *J. Chem. Phys.* **90**, 91 (1989).
- 6) A.V. Dentamaro and D.H. Katayama, "Collisional deactivation of the isoelectronic $^{15}N_2^+$ $A^2\Pi_{ui}$ ($v=3$) and CO^+ $A^2\Pi_i$ ($v=3$ and 4) levels by helium atoms," *J. Chem. Phys.* **101**, 8628 (1994).
- 7) W.J. Marinelli, W.J. Kessler, B.D. Green and W.A.M. Blumberg, "Quenching of N_2 ($a^1\Pi_g$, $v=0$) by N_2 , O_2 , CO , CO_2 , CH_4 , H_2 , and Ar," *J. Chem. Phys.* **90**, 2167 (1989).
- 8) G. Sha, D. Proch and K.L. Kompa, "Rovibronic energy transfer from N_2 ($a^1\Pi_g$) to CO ($A^1\Pi$) studied by laser REMPI spectroscopy," *J. Chem. Phys.* **87**, 2742 (1987).
- 9) G. Sha, D. Proch and K.L. Kompa, "Rotational transitions of N_2 ($a^1\Pi_g$) induced by collisions with Ar/He and N_2 ($a^1\Pi_g$) - N_2 ($X^1\Sigma_g^+$) rovibronic energy transfer studied by laser REMPI spectroscopy," *J. Chem. Phys.* **87**, 5251 (1987).
- 10) D.H. Katayama and A.V. Dentamaro, "Direct observation of collision induced transitions between the $a^1\Pi_g$ ($v=0$) and $a^1\Sigma_u^-$ ($v=0$) levels of N_2 via double resonance enhanced multi-photon ionization spectroscopy," *J. Chem. Phys.* **97**, 2820 (1992).
- 11) D.H. Katayama, A.V. Dentamaro and J.A. Welsh, "State specific electronic quenching rates for the N_2 $a^1\Pi_g$ ($v'=0$) level from collisions with He, Ar, and N_2 ," *J. Chem. Phys.* **101**, 9422 (1994).

- 12) D.H. Katayama, A.V. Dentamaro and J.A. Welsh, Collision-induced electronic transitions from the N_2 $a^1\Pi_g$ ($v' = 1$ and 2) levels," *J. Phys. Chem.* **100**, 7854 (1996).
- 13) H.-M. Lin, M. Seaver, K.T. Yang, A.E.W. Knight and C. Parmenter, "The role of intermolecular potential well depths in collision-induced state changes," *J. Chem. Phys.* **70**, 5442 (1979).

7 PUBLICATIONS

- 1) "Collisional deactivation of the isoelectronic $^{15}N_2^+$ $A^2\Pi_{ui}(v=3)$ and CO^+ $A^2\Pi_i(v=3$ and $4)$ levels by helium atoms," A.V. Dentamaro and D.H. Katayama, *J. Chem. Phys.* **101**, 8628 (1994).
- 2) "State specific electronic quenching rates for the N_2 $a^1\Pi_g(v'=0)$ level from collisions with He, Ar and N_2 ," D.H. Katayama, A.V. Dentamaro and J.A. Welsh, *J. Chem. Phys.* **101**, 9422 (1994).
- 3) "Collision induced electronic transitions from the N_2 $a^1\Pi_g(v=1$ and $2)$ levels," D.H. Katayama, A.V. Dentamaro and J.A. Welsh, *J. Phys. Chem.* **100**, 7854 (1996).
- 4) "Collision Induced Transitions Between the $a^1\Pi_g$, $a^1\Sigma_u^-$ and $w^1\Delta_u$ States of N_2 : Can They Affect Auroral N_2 Lyman-Birge-Hopfield Band Emissions?," R.W. Eastes and A.V. Dentamaro, *J. Geophys. Res.* **101**, 26931 (1996).

8 MEETINGS

- 1) "Collision Induced Electronic and Rotational Transitions from Selectively Excited States of the N_2 $a^1\Pi_g$ State," A.V. Dentamaro and D.H. Katayama, 1993 Meeting of the Division of Atomic, Molecular and Optical Physics, 16-19 May 1993, Reno, NV.
- 2) "Laser Double Resonance Experiments in the Study of the Collisional Effects on the Atmospheric LBH Emissions," A.V. Dentamaro and D.H. Katayama, 11th Interdisciplinary Laser Science Conference, 10-15 Septemeber 1995, Portland, OR.
- 3) "Collision Induced Electronic Transitions Between the $a^1\Pi_g$, $a^1\Sigma_u^-$ and $w^1\Delta_u$ States of N_2 ," A.V. Dentamaro and D.H. Katayama, 1996 Meeting of the Division of Atomic, Molecular and Optical Physics Annual Meeting, 15-18 May 1996, Ann Arbor, MI.

(This page intentionally left blank)

CHARACTERIZATION OF UV EMISSIONS RESULTING FROM ELECTRONIC ENERGY TRANSFER IN ATMOSPHERIC MOLECULES

Abstract

We report branching fraction measurements for the energy transfer reactions $N_2(A^3\Sigma_u^+, v')$ + $NO(X^2\Pi_r, v''=0) \rightarrow N_2(X^1\Sigma_g^+, v'')$ + $NO(A^2\Sigma^+, v' \leq 1)$ + $NO(B^2\Pi_r, v'=0)$ and $CO(a^3\Pi, v' \leq 3)$ + $NO(X^2\Pi_r, v''=0) \rightarrow CO(X^1\Sigma^+, v'')$ + $NO(A^2\Sigma^+, v' \leq 2)$ + $NO(B^2\Pi_r, v'=0)$. In addition we discuss the $N(^4S) + NO(X^2\Pi_r)$ product channel measured in the reaction $N_2(A^3\Sigma_u^+, v') + O(^3P)$.

1 INTRODUCTION

In recent years, there has been an increased interest in the use of remote sensing techniques in the ultraviolet and visible regions of the electromagnetic spectrum to characterize 'active' environments such as naturally occurring 'auroras' and man-made 'plasmas'. The results of these optical measurements are then interpreted using complex computer models based on known kinetic processes. It becomes obvious that there is a dire need to characterize the basic energy transfer and reactive pathways for these collision processes that involve simple neutrally charged diatomic species, *i.e.*, measure vibrational level specific bimolecular rate constants and product channel distributions as a function of vibrational energy in the precursor state, using experimental techniques that are free of competing processes and provide the direct monitoring of the states of interest, *i.e.*, minimize the use of sensitized emission techniques whenever possible.

Presented below is a summary of the experimental measurements that were conducted in the UV Gas Phase Kinetics Laboratory from November 1993 through March 1997. These investigations were designed to characterize energy transfer processes of simple diatomic molecules, *e.g.*, $N_2(A^3\Sigma_u^+)$ and $CO(a^3\Pi)$, that are known to play an important role¹ in the 'chemistry' of 'normal' and 'perturbed' environments, *e.g.*, auroras and plasmas. These long lived electronically excited species are known to be the precursor states for many short lived emitting states, *e.g.*, $NO(A^2\Sigma^+)$ and $NO(B^2\Pi_r)$, whose emissions are being used to model the complex environments of rocket motor exhausts and more recently, emissions emanating from the surfaces of re-entry vehicles and other blunt objects traversing the atmosphere.

The characterization of the 'reactivity' of the lowest lying electronically excited state of molecular nitrogen, the $N_2(A^3\Sigma_u^+)$ state, has been the subject of many investigations over the past 25 years. A recent review article by Golde⁸ provides an excellent discussion of these measurements. Many of the previous measurements, with the exception of the measurements performed by Dreyer *et al.*⁹⁻¹¹ who used complex absorption techniques to measure the vibrational level specific bimolecular rate constants, were accomplished using $N_2(A^3\Sigma_u^+)$ Hg I or $NO(A^2\Sigma^+, v' \rightarrow X^2\Pi_r, v'')$ γ bands sensitized emission techniques to monitor the relative concentration of the $N_2(A^3\Sigma_u^+)$, i.e., $N_2(A^3\Sigma_u^+) + NO(X^2\Pi_r) \rightarrow N_2(X^1\Sigma_g^+, v'') + NO(A^2\Sigma^+, v')$ followed by emission from the $NO(A^2\Sigma^+, v' \rightarrow X^2\Pi_r, v'')$ γ bands. Recently, Piper *et al.*³ has shown that rate constants measured using Hg I or $NO(A^2\Sigma^+, v' \rightarrow X^2\Pi_r, v'')$ γ bands sensitized emissions are sensitive to the vibrational level population distribution of the electronically excited precursor state when the vibrational levels of the electronically excited state are quenched with different efficiencies, i.e., the measured rate constant will be an average value dependent on the precursor state's vibrational level population distribution and relative quenching rates,

$$k_{measured} = \sum_{v_{min}}^{v_{max}} f_v \cdot k_v, \text{ where } f_v \text{ is the fraction of the precursor state's that is in a given}$$

vibrational level, v , k_v is the actual bimolecular rate constant for v and $1 = \sum_{v_{min}}^{v_{max}} f_v$.

The lowest lying electronically excited state of carbon monoxide, the $CO(a^3\Pi)$, is energy rich¹² with ~6.0 eV in $v'=0$ (Figure 2)¹³ and radiative lifetime of ~9.5 ms¹². The room temperature vibrational level specific bimolecular rate constants for the electronic quenching of the $CO(a^3\Pi)$ state in $v' \leq 4$ have been reported previously¹⁴⁻¹⁷. Very good agreement is found between these investigations for the colliders that were investigated. Contrary to the behavior observed in the electronic quenching of the $N_2(A^3\Sigma_u^+)$ state, discussed below, the $CO(a^3\Pi, v')$ electronic

quenching shows little dependence on vibrational quanta in the $\text{CO}(a^3\Pi)$ state, at least for the colliders investigated.

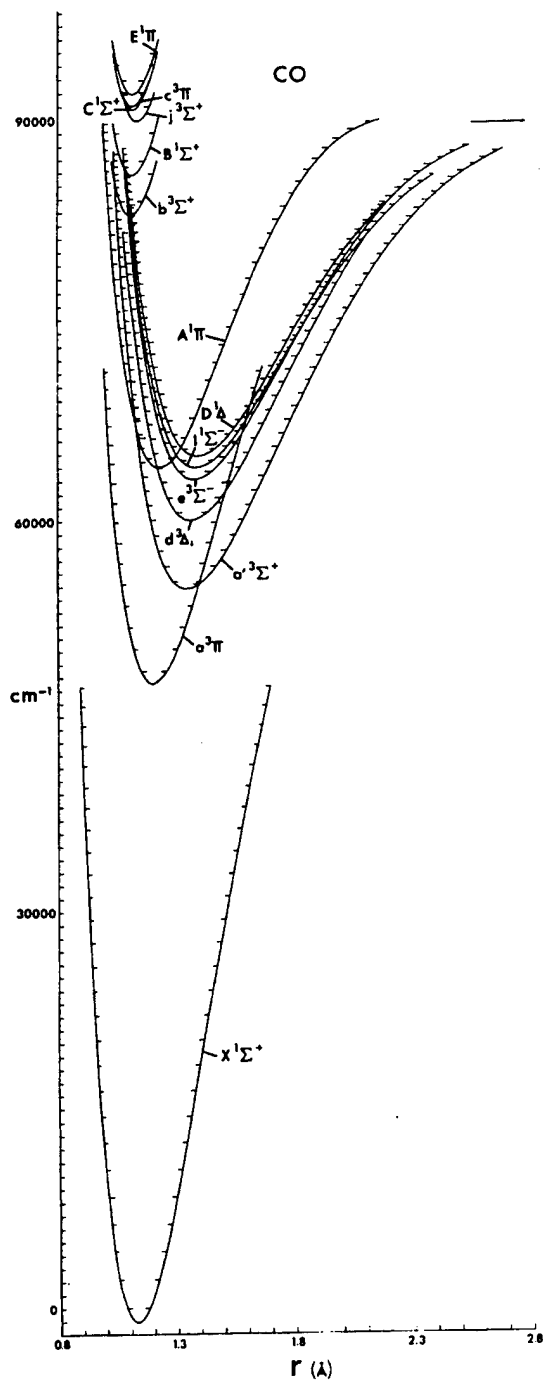


Figure 2. Potential energy curves for carbon monoxide from S. G. Tilford and J. D. Simmons, *J. Chem. Phys. Ref. Data 1* (1972) 1.

The excitation of the $\text{NO}(A^2\Sigma^+)$ and $\text{NO}(B^2\Pi_r)$ states continues to be of interest to many modelers because they are used as precursor states to "signature" emissions for many energy transfer processes. The potential energy curves for nitrogen monoxide are presented in Figure 3.^{18,19} The emissions from the $\text{NO}(A^2\Sigma^+, v' \rightarrow X^2\Pi_r, v'')$ γ bands or $\text{NO}(B^2\Pi_r, v' \rightarrow X^2\Pi_r, v'')$ β bands and the intensity ratios of these emissions can be used to characterize the long-lived, weakly emitting precursor states present in the "active" environments. The vibrational level specific bimolecular rate constants for the energy transfer reaction $\text{N}_2(A^3\Sigma_u^+, v') + \text{NO}(X^2\Pi_r, v'' = 0)$ have been measured previously^{3,10,20,21}. There exist additional measurements reported in the literature⁸ but these were measured using indirect sensitized emission techniques that are affected by the vibrational population distribution of the $\text{N}_2(A^3\Sigma_u^+)$ state. A summary of the measurements reported by Thomas^{20,22-25} is presented in Figure 4. It can be seen in Figure 4 that while some of the $\text{N}_2(A^3\Sigma_u^+)$ electronic quenchers show little or no dependence on vibrational level in the $\text{N}_2(A^3\Sigma_u^+)$ state, e.g., $\text{N}_2(A^3\Sigma_u^+, v') + \text{NO}(X^2\Pi_r)$, some quenchers show a marked dependence on vibrational level in the $\text{N}_2(A^3\Sigma_u^+, v)$, e.g., $\text{N}_2(A^3\Sigma_u^+, v') + \text{CO}(X^1\Sigma^+, v'' = 0)$. The reason for this dependence is discussed elsewhere^{10,20,25}.

Discussed below are the results of two main projects that were undertaken while this contract was in place, i.e., "Branching fractions of the product $\text{NO}(A^2\Sigma^+, v' = 0$ and 1) and $\text{NO}(B^2\Pi_r, v' = 0)$ emissions observed as a function of v' in the energy transfer reaction $\text{N}_2(A^3\Sigma_u^+, v') + \text{NO}(X^2\Pi_r)$ " and "Branching fractions of the product $\text{NO}(A^2\Sigma^+, v' = 0, 1, \text{ and } 2)$ and $\text{NO}(B^2\Pi_r, v' = 0)$ emissions observed as a function of v' in the energy transfer reaction $\text{CO}(a^3\Pi, v' \leq 4) + \text{NO}(X^2\Pi_r, v'' = 0)$." In addition, enhancements and modifications

made to the data acquisition software and data analysis software during the past several years will be discussed briefly.

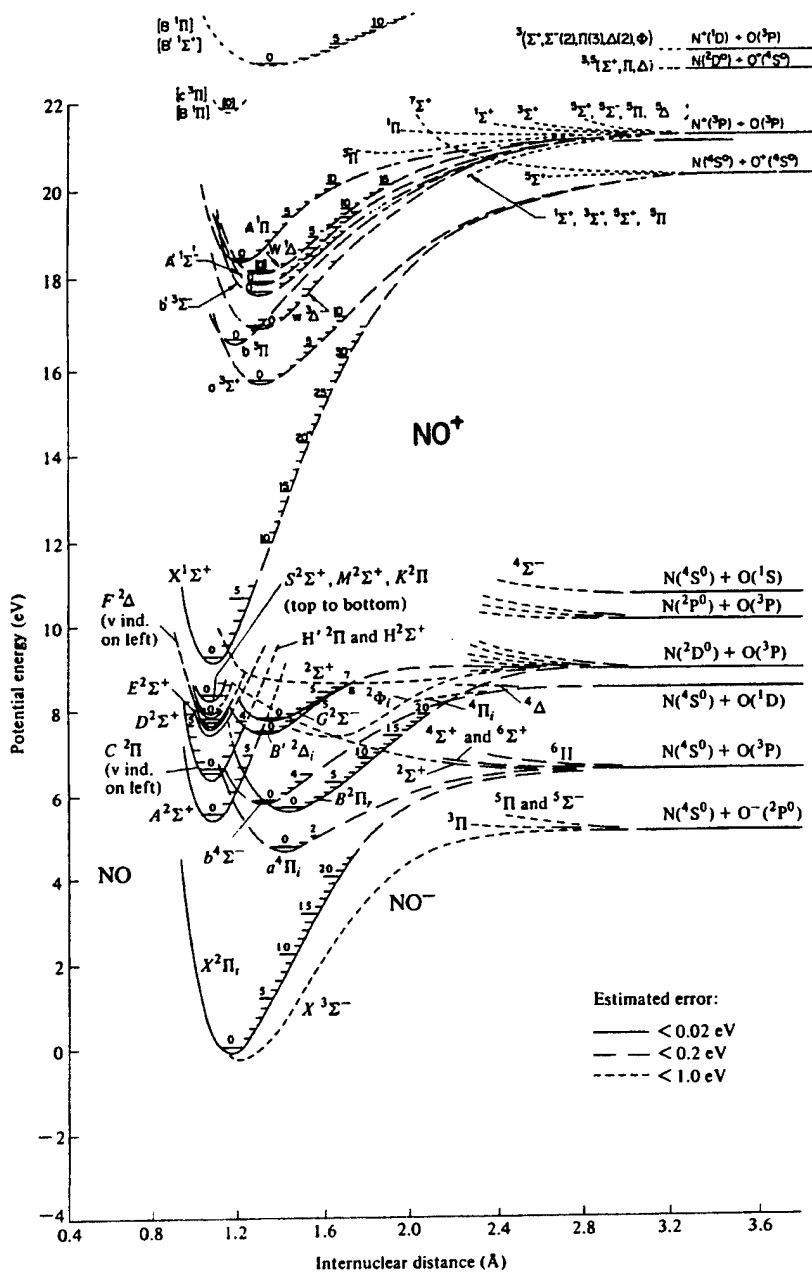


Figure 3. Potential energy curves for nitrogen monoxide from F. R. Gilmore, Rand Corporation Memorandum R-4034-PR (June 1964).

N₂(A,v') Modified Power Law Plot

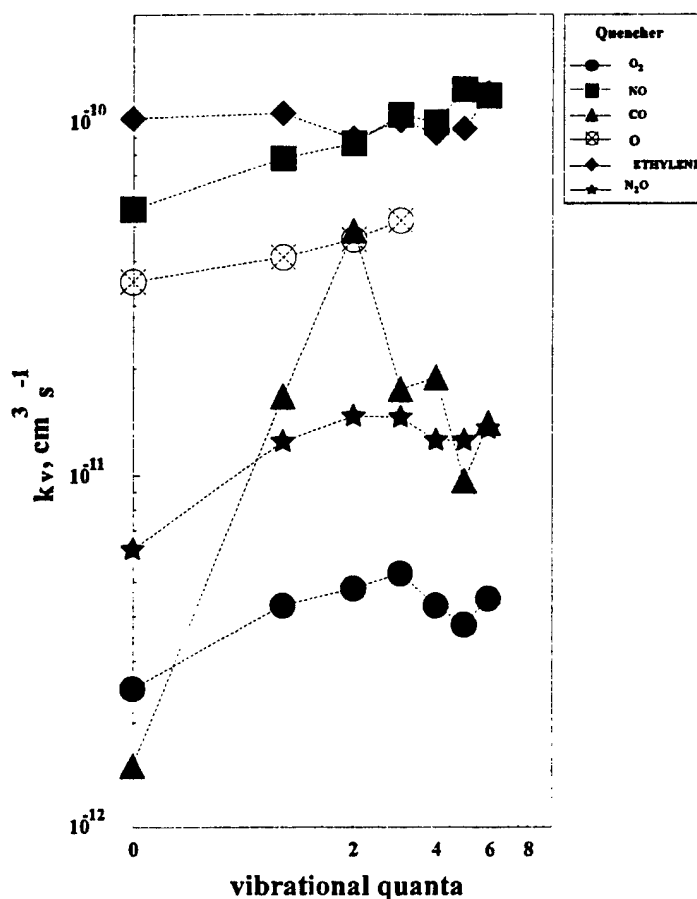


Figure 4. Summary of the N₂ A+Q, rate constant measurements presented in Modified power law form, $\ln k$ vs $n \ln(v + 1/2)$ from J.M. Thomas, Ph.D. Thesis, University of Pittsburgh, 1986.

A third project is discussed. Although the experimental work was performed previously²⁵ it was never written up in manuscript form. Recent efforts to model perturbed environments by Bose and Candler²⁶⁻²⁹ suggest that the ground state of molecular nitrogen in highly vibrationally excited states, i.e., N₂(X ¹Σ_g⁺, v'' > 0), reacting with atomic oxygen, O(³P), is a significant source of nitric oxide, NO(X ²Π_g). Our measurements³⁰ have shown that the NO + N product channel in the energy transfer reaction N₂(A ³Σ_u⁺, v') + O(³P) is not a significant source of NO at room temperature.

2 EXPERIMENTAL

The rapidly pumped discharge-flow reactor used over the past several years to characterize the $N_2(A^3\Sigma_u^+)$ and $CO(a^3\Pi)$ states has been described in detail previously.²¹ A representative rapidly pumped discharge-flow reactor configuration is presented in Figure 5. As before,²¹ two basic flow-tube configurations are utilized to determine the sensitivity of the product emissions to $N_2(A^3\Sigma_u^+, v')$ and $CO(a^3\Pi, v')$. The ratios of the product emissions are found to be insensitive to flow-tube configuration and a majority of the experimental measurements are made using the straight flow-tube configuration. $N_2(A^3\Sigma_u^+, v')$ is generated using the well established energy transfer reaction $Ar(^3P_{2,0}) + N_2(X^1\Sigma_g^+, v''=0)^{31,32}$. N_2 is added immediately downstream (~ 2 ms) of the low power (~ 300 V, ~ 1.0 mA) dc discharge in Ar where the $Ar(^3P_{2,0})$ metastables are produced. The major product of the energy transfer reaction $Ar(^3P_{2,0}) + N_2(X^1\Sigma_g^+, v''=0)$ is $N_2(C^3\Pi_u, v' \leq 3)^{32}$. Radiative and collisional deactivation in the triplet manifold of N_2 leads to the formation of $N_2(A^3\Sigma_u^+, v')$.

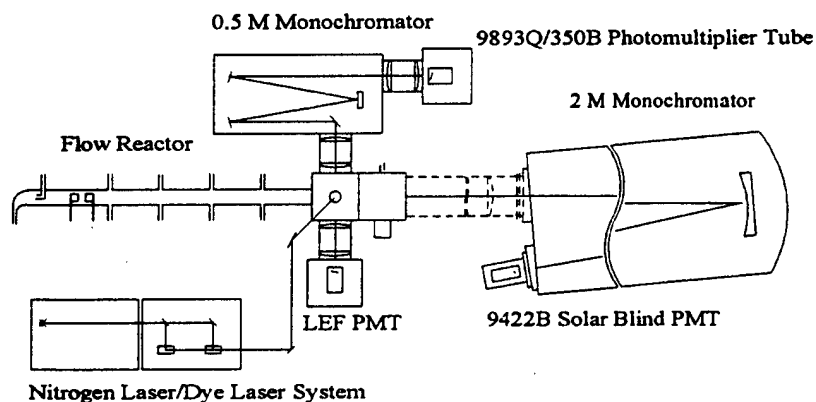


Figure 5. Schematic diagram of the rapidly pumped discharge-flow reactor used in the present investigations.

The $N_2(A^3\Sigma_u^+, v')$ population distribution is controlled using two techniques. First, the $N_2(A^3\Sigma_u^+, v')$ population distribution is known to be sensitive to the total $[N_2(X^1\Sigma_g^+)]$. The

$[N_2(A^3\Sigma_u^+, v' \geq 2)]$ is inversely proportional $[N_2(X^1\Sigma_g^+)]$.³³ Work reported by Dreyer and Perner⁹ suggests that $N_2(X^1\Sigma_g^+)$ vibrationally relaxes $N_2(A^3\Sigma_g^+, v')$ in $\Delta v = v' - v'' = 2$ increments. When the N_2 flow is ~20% of the total flow (~2 Torr Ar), only $N_2(A^3\Sigma_u^+, v' \leq 2)$ is detected in the observation region using laser-excited fluorescence techniques. Under these flow conditions, the population distribution of the $N_2(A^3\Sigma_u^+, v')$ in the observation region or the rapidly pumped discharge-flow reactor is 1.00 : 0.66 : 0.28 for $v'=0, 1$ and 2, respectively. By reducing the N_2 flow to ~0.5% of the total flow, $N_2(A^3\Sigma_u^+, v' \leq 6)$ can be detected in the observation region using laser-excited fluorescence detection techniques. Second, some inefficient $N_2(A^3\Sigma_u^+)$ electronic quenchers, e.g., CH_4 and CF_4 , designated Q_v , have been observed to vibrationally relax the upper v' levels into the $v'-1$ level.^{17,22} By using excess $[Q_v]$ all of the $N_2(A^3\Sigma_u^+)$ state population can be relaxed into $v'=0$. By varying the $[N_2]$, Q_v and $[Q_v]$, product branching ratios can be mapped as a function of initial $N_2(A^3\Sigma_u^+, v')$ population distribution. Both techniques are used in the present investigation. The extent of relaxation that occurred by the time the $N_2(A^3\Sigma_u^+, v')$ reached the observation region is measured directly by monitoring the spontaneous emission from the 0,4 transition of the $N_2(A^3\Sigma_u^+, v' \rightarrow X^1\Sigma_g^+, v'')$ Vegard-Kaplan bands, and probing the 4,0 and 5,1 transitions of the $N_2(B^3\Pi_g^-, v' - A^3\Sigma_u^+, v'')$ First Positive bands using laser-excited fluorescence techniques. From previous work^{22,25,33}, we know that under the flow conditions used in the present experiment that the ratio of $v'=1 : v'=2$ is ~1.00 : 0.42.

The $[N_2(A^3\Sigma_u^+, v'=0 \text{ and } 1)]_{\text{RELATIVE}}$ is detected at the first observation port on the upstream detection cell utilizing laser-excited fluorescence techniques. Tunable radiation from a nitrogen laser pumped dye laser system (Molelectron, Models UV-24 and DL-II, respectively) is used to

excite the 4,0 and 5,1 transitions of the $N_2(B^3\Pi_g, v' - A^3\Sigma_u^+, v'')$ First Positive bands at the P_1 band heads. Fluorescence to the red of the excitation radiation is collected using a dry-ice cooled red-sensitive photomultiplier tube (Hamamatsu, Model 943-02). Scattered light from the excitation radiation is attenuated using sharp cutoff filters (Corning, CS 2-58 and 2-59) and pulse-pile up problems are eliminated using a neutral density filter (Schott, NG-5) to reduce the intensity of the emission signal. The $[N_2(A^3\Sigma_u^+, v'=0)]_{RELATIVE}$ is detected using a second technique. Emission from the 0,4 transition of the $N_2(A^3\Sigma_u^+, v' \rightarrow X^1\Sigma_g^+, v'')$ Vegard-Kaplan bands is measured using a Thorn/EMI solar blind photomultiplier tube (Model 9422B) attached to a 0.5 m grating spectrophotometer (Spex, Model 1870). The width of the entrance and exit slits on the 0.5 m grating spectrophotometer is set to 100 microns. The height of the entrance slit is set to 2 mm. The sensitivity of the detection system is calibrated using the technique described by Mumma and Zipf³⁴ and Mumma³⁵.

In determining the relative population distribution of the $N_2(A^3\Sigma_u^+)$ state in the observation region, consideration must be given to the effect of the electronic quenching of the $NO(X^2\Pi_r, v''=0)$ on the $N_2(A^3\Sigma_u^+, v')$ population distribution. The $[NO(X^2\Pi_r, v''=0)]$ is optimized for maximum signal. Under our flow conditions this is $\sim 4.0 \times 10^{12}$ molecules cm^{-3} . If the rate constants for the electronic quenching of the $N_2(A^3\Sigma_u^+, v')$ by $NO(X^2\Pi_r, v'')$ showed no vibrational level dependence, the relative population distribution would be insensitive to $NO(X^2\Pi_r, v'')$ additions. An enhancement in the vibrational level specific bimolecular rate constant, k_v (cm^3 molecules $^{-1}$ s $^{-1}$), has been reported^{10,20} for the energy transfer reaction $N_2(A^3\Sigma_u^+, v') + NO(X^2\Pi_r, v''=0)$. Using the data reported by Thomas et al.²⁰ we obtain first-order removal rates, i.e., $k_v \times [NO(X)]$ (s $^{-1}$), of 224, 312, and 344 for $v'=0, 1$ and 2 , respectively. In the 0.0037 s residence time (corrected for flow dynamics^{36,37}) between NO addition and product emission detection, the $N_2(A^3\Sigma_u^+, v'=0, 1$ and $2)$ will be reduced by a

factor of 0.437, 0.315, and 0.280 for $v'=0, 1$ and 2 , respectively. Using this information, we can determine the corrected vibrational level population distribution in the observation region after NO is added. For the $N_2(A^3\Sigma_u^+, v'=0)$ measurements no correction is necessary. For the $N_2(A^3\Sigma_u^+, v' \leq 1)$ measurements we obtain a population ratio of $1.00 : 0.08$ for $v'=0$ to 1 , respectively. For the $N_2(A^3\Sigma_u^+, v' \leq 2)$ measurements we obtain a corrected population distribution of $1.00 : 0.29 : 0.11$ for $v' = 0 : 1 : 2$, respectively.

$CO(a^3\Pi, v')$ is generated using one of four energy transfer reactions^{15,17,38,39}: $Ar(^3P_{2,0}) + CO_2(X^1\Sigma_g^+)$, $Ar(^3P_{2,0}) + CO_2(X^1\Sigma_g^+)/CO(X^1\Sigma^+)$, $He(^3S_1) + CO_2(X^1\Sigma_g^+)/CO(X^1\Sigma^+)$ and $He(^3S_1) + CO_2(X^1\Sigma_g^+)/SF_6$. Each energy transfer reaction provides a different nascent $CO(a^3\Pi)$ vibrational level population distribution. A summary of the $CO(a^3\Pi, v')$ population distributions for each of these reactions is presented in Table 1. The relative populations are calculated using the standard equation for emission intensity⁴⁰ described below. The generating reaction $Ar(^3P_{2,0}) + CO_2(X^1\Sigma_g^+)$ produces $CO(a^3\Pi)$ primarily in $v'=0$ ³⁹ as only $\sim 1.6\%$ of the $CO(a^3\Pi)$ population is in $v'=1$. The generating reaction $He(^3S_1) + CO_2(X^1\Sigma_g^+)$ yields the most unrelaxed $CO(a^3\Pi, v')$ distribution. We used a $1:1$ mixture of $CO_2(X^1\Sigma_g^+)$ in $CO(X^1\Sigma^+)$ to obtain the two intermediate $CO(a^3\Pi)$ vibrational level population distributions as shown in Table 1.

$Ar(^3P_{2,0})$ and $He(^3S_1)$ metastables are generated in a low power (~ 300 V, ~ 1 mA) dc discharge tube (Yankee Glassblowers, Concord MA) in Ar or He, respectively. $CO_2(X^1\Sigma_g^+)$ or the $\sim 1:1$ $CO_2(X^1\Sigma_g^+)/CO(X^1\Sigma^+)$ mixture is added immediately downstream (~ 2 ms) of the metastable generation region at the precursor inlet system. SF_6 is added to the flow at the

precursor inlet system when He metastables are used to generate the $\text{CO}(a^3\Pi)$ to quench unwanted CO^* emissions^{17,38}. A buffer flow of Ar or He is used to ensure rapid mixing at the precursor and reactant inlet systems.

Table 1: $\text{CO}(a^3\Pi, v')$ Nascent Population Distributions^a

Generating Reaction ^b	$v' = 0$	$v' = 1$	$v' = 2$	$v' = 3$
$\text{Ar}^* + \text{CO}_2$	0.984 ± 0.000	0.016 ± 0.003		
$\text{Ar}^* + \text{CO}/\text{CO}_2$	0.822 ± 0.048	0.143 ± 0.009	0.026 ± 0.009	0.009 ± 0.001
$\text{He}^* + \text{CO}/\text{CO}_2/\text{SF}_6$	0.670 ± 0.102	0.167 ± 0.026	0.099 ± 0.016	0.064 ± 0.011
$\text{He}^* + \text{CO}_2/\text{SF}_6$	0.476 ± 0.021	0.270 ± 0.013	0.164 ± 0.008	0.090 ± 0.007

a) The relative intensities were calculated using the equation for N_v (See text for discussion) with $R_e = 1$ and emission signal from the CO a-X Cameron $v' = 0, 1, 2$ and 3 , $\Delta v = v' - v'' = -2, -3$ and -4 bands. The uncertainties reported in the table account for the statistical uncertainty (1σ) associated with the measurements. An additional 12% should be added in quadrature to the above uncertainties to account for the total experimental uncertainty.

b) Ar or He metastables were generated using a low power d.c. discharge in Ar or He. See text for discussion.

Emission from the $\text{CO}(a^3\Pi, v'=0-3 \rightarrow X^1\Sigma^+, v'')$ Cameron, $\Delta v = v' - v'' = -2, -3$ and -4 bands (Figure 6), $\text{NO}(A^2\Sigma^+, v'=0-2 \rightarrow X^2\Pi_r, v'')$ γ , $\Delta v = -4, -5$, and -6 bands and $\text{NO}(B^2\Pi_r, v'=0 \rightarrow X^2\Pi_r, v'')$ β , $\Delta v = -6$ and -7 bands (Figure 7) is measured using a solar blind photomultiplier tube (Thorn/EMI model 9422B) attached to a 0.5 m grating spectrophotometer (Spex, model 1870). The width of the entrance and exit slits on the 0.5 m grating spectrophotometer is set to 100 μm . The height of the entrance slit is set to 2 mm. The relative sensitivity of the detection system is calibrated using the technique described by Mumma and Zipf³⁴ and Mumma³⁵.

All photoelectric emission measurements are acquired using photon counting techniques. Output from the photomultiplier tube is passed through a pulse amplifier discriminator (Pacific Instruments, model AD6 or SpaCom Electronics, model 135A). The output of the pulse amplifier discriminator is accumulated on a counter/timer (Tennelec, model TC-535P). Data acquisition is controlled using a ZDS/Bull 248 (AT compatible) computer system and data

analysis is performed on either a DELL 386SX/16 or Packard Bell 486DX/66 Force 203 computer. Software developed using Microsoft's BASIC Professional Development System v7.1 (*tm*) or Microsoft's Visual BASIC v3.0 and libraries contained in Crescent Software's QuickPak Professional (*tm*) are used to collect and analyze the photoelectric emission spectra. The reported uncertainties account for the statistical uncertainties (1σ) associated with the measurements^{41,42}. The systematic uncertainty is estimated to be $\sim 12\%$ and unless otherwise noted should be added in quadrature to the reported uncertainties to obtain an estimate of the total experimental uncertainty^{41,42}.

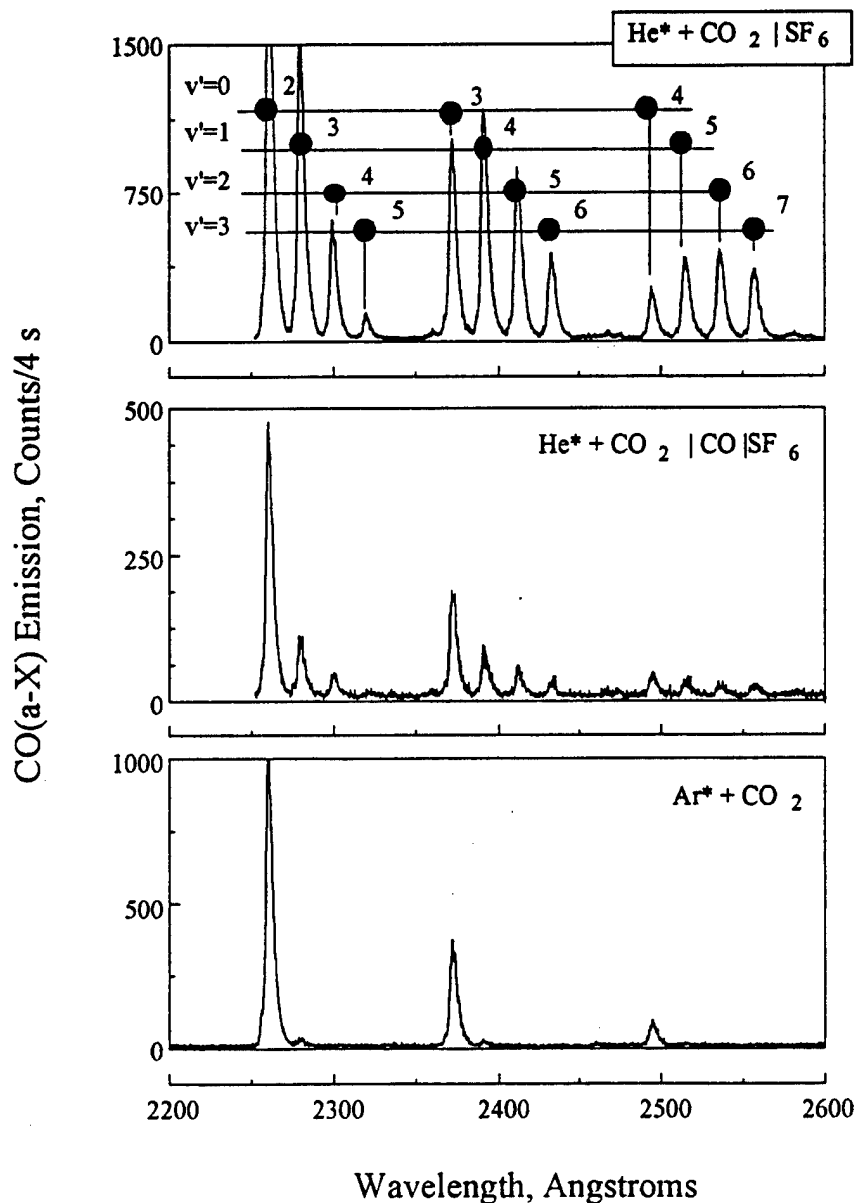


Figure 6. Photoelectric emission spectra for the CO a-X Cameron bands obtained from three of the four generating reactions used.

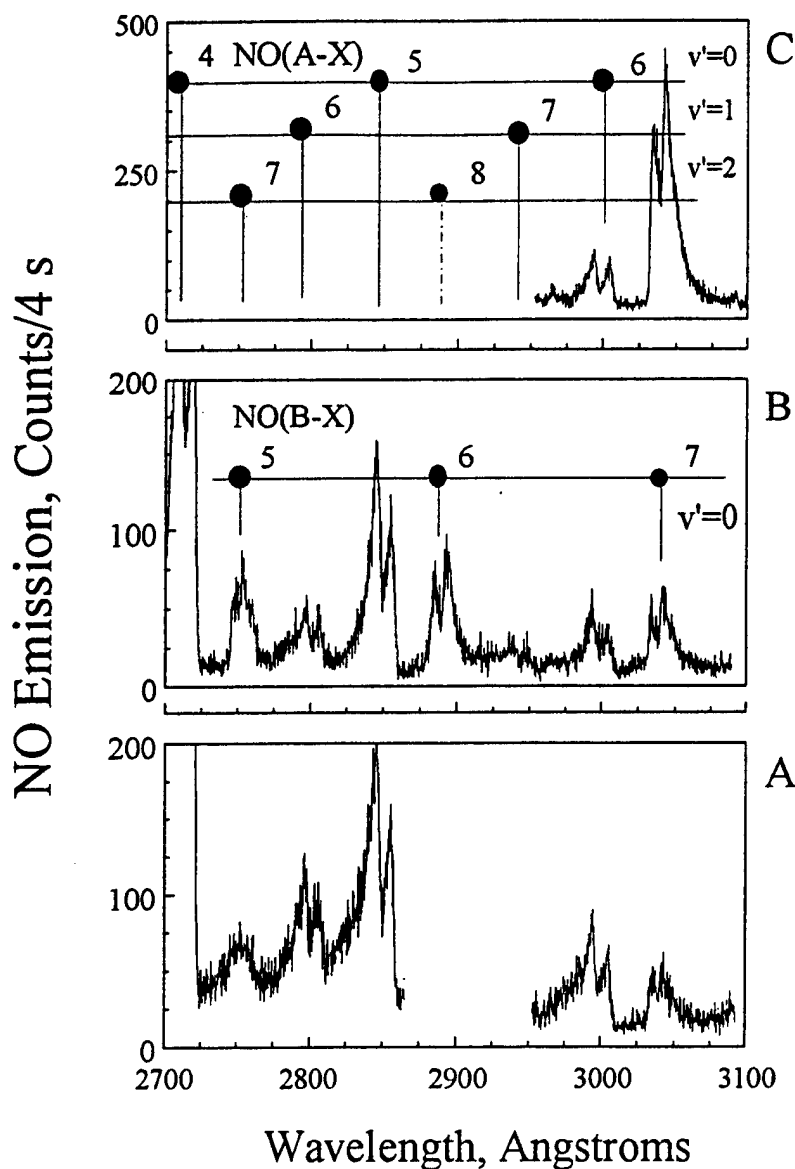


Figure 7. Photoelectric emission spectra for the energy transfer reaction $\text{CO}(a, v') + \text{NO}(X, v''=0) \rightarrow \text{CO}(X, v'') + \text{NO}(A, v') + \text{NO}(B, v')$. See text for discussion.

Ar (Matheson, 99.999%) and N_2 are obtained in liquid form and stored in a high-pressure (~200 psig) dewars (MVE Cryogenics, DuraCyl). Boil-off from the liquid reservoirs is used as the source for the gas flows. He (US Bureau of Mines, High Purity, 99.995%) is obtained in 1A cylinders. Oxidizable contaminants are removed from the Ar, N_2 and He using a Cu packed quartz furnace (~800 K) located on the high pressure side of the gas delivery system. Condensable impurities are removed from the main Ar and He flows by passing the Ar and He through a series of four (4) molecular sieve packed traps (Fisher Scientific, Type 4A Grade 514, 8-12 mesh) immersed in liquid N_2 (77 K) on the low-pressure side of the gas delivery system. An additional trap located on the high pressure side of the gas delivery system is used to further reduce the

condensable impurities when He is used as the main carrier gas. CO₂ (Air Products, Coleman grade 99.99%) is purified using a series of three (3) freeze-pump-thaw cycles and stored in two (2) five liter Pyrex bulbs. The NO/He (Matheson, Analyzed 10.3%), CO (Matheson, Research Grade 99.99%) and SF₆/He (Air Products, Analyzed 0.992%) are used without further purification. A 1% mixture (NO/He) was prepared from the 10.3% mixture using standard gas handling techniques and stored in a five liter Pyrex bulb. CH₄ (Matheson, UHP, 99.97%), CF₄ (Matheson, 99.9%), and NO/He (Matheson, Analyzed) mixture are used without further purification.

3 RESULTS AND DISCUSSION.

3.1 BRANCHING FRACTIONS OF THE PRODUCT NO(A ²Σ⁺, v'=0 and 1) AND NO(B ²Π_r, v'=0) EMISSIONS OBSERVED AS A FUNCTION OF v' IN THE ENERGY TRANSFER REACTION N₂(A ³Σ_u⁺, v') + NO(X ²Π_r, v''=0).

A series of photoelectric emission spectra is presented in Figure 8 for the energy transfer reactions N₂(A ³Σ_u⁺, v' =0) + NO(X ²Π_r, v''=0) (Figure 8-1), N₂(A ³Σ_u⁺, v' ≤1) + NO(X ²Π_r, v''=0) (Figure 8-2), N₂(A ³Σ_u⁺, v' ≤2) + NO(X ²Π_r, v''=0) (Figure 8-3), and N₂(A ³Σ_u⁺, v' ≤ 6) + NO(X ²Π_r, v''=0) (Figure 8-4). For completeness, a background emission spectrum is presented in the lower portion of Figure 8-1. Emission is observed from the 0,7 and 0,8 transitions of the NO(B ²Π_r, v' - X ²Π_r, v'') β bands and the 0,7 and 1,8 transitions of the NO(A ²Σ⁺, v' - X ²Π_r, v'') γ bands at 3,035.3, 3,198.6, 3,158.2, 3,093.6 Å, respectively (Figures 8-1 through 8-4). Although both the NO(A ²Σ⁺, v' - X ²Π_r, v'') γ bands and NO(B ²Π_r, v' - X ²Π_r, v'') β bands have two pronounced band heads, they are easily distinguishable from each other because of their opposite shading directions. A dramatic increase in the intensity of the 0,7 and 0,8 transitions of the NO(B ²Π_r, v' - X ²Π_r, v'') β bands is observed as the v' = 1 and 2 vibrational levels of the N₂(A ³Σ_u⁺) state are populated. Similarly, emission from the 1,8 transition of the NO(A ²Σ⁺, v' - X ²Π_r, v'') γ bands is observed to increase with v' in an analogous manner. The intensities of the emissions from the NO(A ²Σ⁺, v' - X ²Π_r, v'') γ bands and NO(B ²Π_r, v' - X ²Π_r, v'') β bands for the

$N_2(A^3\Sigma_u^+, v' \leq 6)$ (Figure 8-4) are slightly larger than that for the $N_2(A^3\Sigma_u^+, v' \leq 2)$ (Figure 8-3).

The emission intensity, $I_{v',v''}$, for a transition from v' to v'' is given by 40

$$I_{v',v''} = \kappa N_{v'} q_{v',v''} v_{v',v''}^3 R_e^3(r_{v',v''}) R_{v',v''} \quad (1)$$

where κ is a constant, $q_{v',v''}$ is the Franck-Condon factor for the v' - v'' transition, $v_{v',v''}$ is the energy for the v' - v'' transition⁴³ in cm^{-1} , $R_e(r_{v',v''})$ is the electronic transition moment, $r_{v',v''}$ is the r -centroid for the v' - v'' transition, and $R_{v',v''}$ is the factor that accounts for the sensitivity of the detection system at the v' - v'' transition. The Franck-Condon factors and the r -centroids for the $\text{NO}(A^2\Sigma^+, v' \rightarrow X^2\Pi_r, v'')$ γ bands and $\text{NO}(B^2\Pi_r, v' \rightarrow X^2\Pi_r, v'')$ β bands are calculated using a technique described by Rabalais⁴⁴ and they are found to be in very good agreement with those reported by Piper and Cowles⁴⁵. $R_e(r_{v',v''})$'s for the $\text{NO}(A^2\Sigma^+, v' \rightarrow X^2\Pi_r, v'')$ γ bands are calculated using an expression reported by Piper and Cowles⁴⁵,

$$R_e(r_{v',v''}) = 33.08 - 58.77 \cdot r_{v',v''} + 26.85 \cdot r_{v',v''}^2 \quad (2)$$

$R_e(r_{v',v''})$'s for the $\text{NO}(B^2\Pi_r, v' \rightarrow X^2\Pi_r, v'')$ β bands are calculated using an expression reported by Piper et al.⁴⁶,

$$R_e(r_{v',v''}) = 0.350 - 0.104 \cdot r_{v',v''} + 3.69 \times 10^4 \cdot e^{-(10.1 \cdot r_{v',v''})} \quad (3)$$

$R_{v',v''}$ is determined using a technique described by Mumma and Zipf³⁴ and Mumma³⁵. $N_{v'}$ is determined by rearranging Eq (1) and κ will be canceled in the determination of the ratios for

$$N_{v'} = \frac{I_{v',v''}}{q_{v',v''} v_{v',v''}^3 R_e^2(r_{v',v''}) R_{v',v''} \kappa} \quad (4)$$

The emission intensity is calculated numerically by integrating the observed emission spectrum, *i.e.*, $I_{v',v''} = \sum_i I_i \delta E_i$, where δE_i is determined using $\frac{E_{i-1} + E_{i+1}}{2}$. The observed wavelengths are

converted to energies using a technique described by Srinivas and Lakshman⁴⁷.

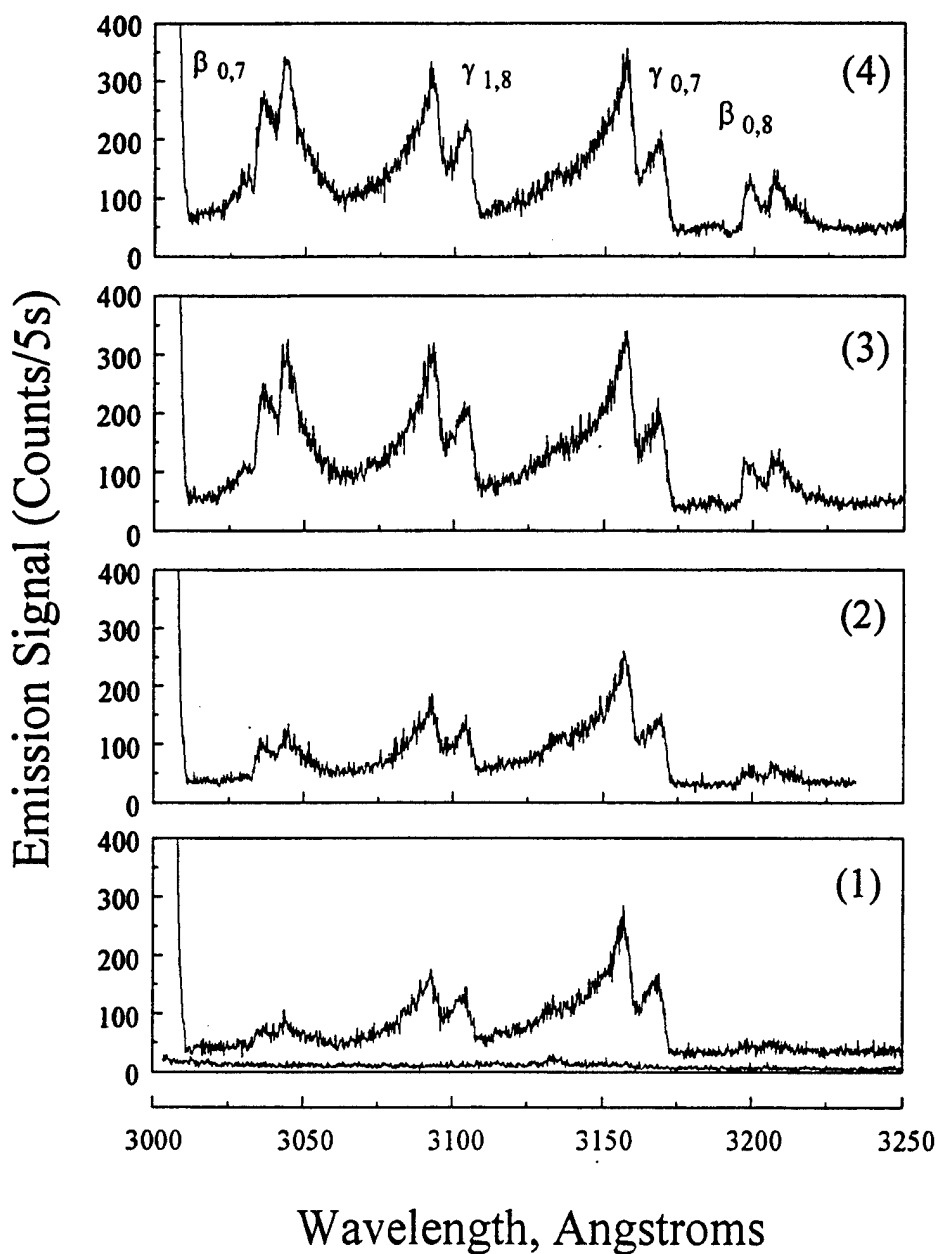


Figure 8. Photoelectric emission spectra for the energy transfer reaction $N_2(A, v') + NO(X, v''=0) \rightarrow N_2(X, v'') + NO(A, v')$. See text for discussion.

From our measurements of the intensities of the 0,7 and 1,8 transitions of the $NO(A^2\Sigma^+, v' - X^2\Pi_r, v'')$ γ bands we obtain a ratio $\frac{[NO(A, v'=0)]}{[NO(A, v'=1)]} = \frac{\gamma_0}{\gamma_1}$ that is obtained using Eq (4). The

other ratios, $\frac{\gamma_0}{\beta_0}$ and $\frac{\gamma_1}{\beta_0}$ are obtained in an analogous manner. The results of these calculations

are presented in Table 2. For the energy transfer reaction $N_2(A^3\Sigma_u^+, v'=0) + NO(X^2\Pi_r, v''=0)$

we observe a ratio $\frac{\gamma_0}{\gamma_1} = (10.1 \pm 1.4) (1\sigma)$. This is in excellent agreement with that reported by Golde and Moyle⁴⁸ who used the 0,0 and 1,0 transitions of the $\text{NO}(A^2\Sigma^+, v' \rightarrow X^2\Pi_r, v'')$ γ bands to obtain this ratio. For an $\text{N}_2(A^3\Sigma_u^+, v' \leq 1)$ population distribution of 1.00 : 0.08 for $v' = 0$ and 1, respectively, we obtain a ratio $\frac{\gamma_0}{\gamma_1}$ of $(8.46 \pm 1.02) (1\sigma)$. We are not aware of any previous measurements reported for this $\text{N}_2(A^3\Sigma_u^+)$ vibrational level population distribution. For an $\text{N}_2(A^3\Sigma_u^+, v' \leq 2)$ population distribution of 1.00 : 0.29 : 0.11 for $v' = 0, 1$ and 2, respectively, in which the N_2 fraction is $\sim 20\%$ of the total flow we find the ratio $\frac{\gamma_0}{\gamma_1}$ to be $(5.74 \pm 0.71) (1\sigma)$, in very good agreement with that reported by Golde and Moyle⁴⁸.

Table 2: Branching ratios of the emission from the NO A-X and B-X bands observed in the energy transfer reaction $\text{N}_2(A, v') + \text{NO}(X, v''=0) \rightarrow \text{N}_2(X, v'') + \text{NO}(A, v') + \text{NO}(B, v'')$ ^a

$\text{N}_2(A, v')$	$\frac{[\text{NO}(A, v'=0)]}{[\text{NO}(A, v'=1)]} = \frac{\gamma_{0,7}}{\gamma_{1,8}}$	$\frac{[\text{NO}(A, v'=0)]}{[\text{NO}(A, v'=1)]} = \frac{\gamma_{0,0}}{\gamma_{1,0}}$	$\frac{[\text{NO}(A, v'=0)]}{[\text{NO}(B, v'=1)]} = \frac{\gamma_{0,7}}{\beta_{0,7}}$	$\frac{[\text{NO}(A, v'=0)]}{[\text{NO}(B, v'=1)]} = \frac{\gamma_{0,7}}{\beta_{0,8}}$	$\frac{[\text{NO}(A, v'=0)]}{[\text{NO}(B, v'=1)]} = \frac{\gamma_{1,8}}{\beta_{1,8}}$
$v' = 0$	10.1 ± 1.44	12.08 (b)	7.67 ± 1.48		
$v' \leq 1^c$	8.46 ± 1.02		3.28 ± 0.42	4.02 ± 0.52	0.75 ± 0.10
$v' \leq 2^d$	5.74 ± 0.71	5.71 (b)	1.54 ± 0.21	1.76 ± 0.25	0.35 ± 0.05

a) The bands used in the determination of the branching ratios are presented in the table for clarity. The reported ratios are obtained using the standard expression for emission intensity (See text for discussion). The uncertainties reported in the table account for both the statistical and systematic uncertainties associated with the measurements. The systematic uncertainty for these measurements is estimated to be $\pm 12\%$.

b) The data in this entry is take from M. F. Golde and A. M. Moyle, Chem. Phys. Letters 117 (1985) 375.

c) The $\text{N}_2(A, v')$ population distribution at the observation region of the rapidly pumped discharge-flow reactor is 1.00 : 0.08 for $v' = 0$ and 1, respectively. See text for discussion.

d) The $\text{N}_2(A, v')$ population distribution at the observation region of the rapidly pumped discharge-flow reactor is 1.00 : 0.29 : 0.11 for $v' = 0, 1$ and 2, respectively. See text for discussion.

The production of the $\text{NO}(B^2\Pi_r)$ state is much more sensitive to the nascent vibrational level population distribution of the $\text{N}_2(A^3\Sigma_u^+)$ state compared to the production of the $\text{NO}(A^2\Sigma^+)$ state. While the γ_1 emission intensity increases by a factor of ~ 2 relative to the γ_0 emission intensity as v' increases from $v'=0$ to $v' \leq 6$ in the $\text{N}_2(A^3\Sigma_u^+)$ state, the β_0 emission intensity is observed to increase by a factor of ~ 5 relative to the γ_0 emission intensity. In the following

discussion, to obtain the ratio $\frac{\gamma_0}{\beta_0}$, we will limit our primary analysis to measurements made

using the 0,7 transition of the $\text{NO}(B^2\Pi_r, v' \rightarrow X^2\Pi_r, v'')$ β bands. We present data in Table 2 for the 0,8 transition of the $\text{NO}(B^2\Pi_r, v' \rightarrow X^2\Pi_r, v'')$ β bands but the reliability of calculations using this band are not as good as those using the 0,7 transition of the $\text{NO}(B^2\Pi_r, v' \rightarrow X^2\Pi_r, v'')$ β bands because of a poorer Signal-to-Noise (See Figure 8) which is the result of the sensitivity of the solar blind photomultiplier tube decreasing rapidly in this wavelength region. For the energy transfer reaction $\text{N}_2(A^3\Sigma_u^+, v'=0) + \text{NO}(X^2\Pi_r, v''=0)$ we determine the ratio $\frac{\gamma_0}{\beta_0}$ using the 0,7

transition of the $\text{NO}(A^2\Sigma^+, v' \rightarrow X^2\Pi_r, v'')$ γ bands and the 0,7 transition of the $\text{NO}(B^2\Pi_r, v' \rightarrow X^2\Pi_r, v'')$ β bands to be (7.67 ± 1.48) (1σ). For the $\text{N}_2(A^3\Sigma_u^+, v' \leq 1)$ population distribution of 1.00 : 0.08 for $v' = 0$ and 1, respectively, we measure a ratio of (3.28 ± 0.42) (1σ) using the same bands, this represents an increase in the $[\text{NO}(B^2\Pi_r, v'=0)]$ of a factor of ~ 2 relative to the $[\text{NO}(A^2\Sigma^+, v'=0)]$ which is significant considering the small percentage of population in the $\text{N}_2(A^3\Sigma_u^+, v'=1)$. For the $\text{N}_2(A^3\Sigma_u^+, v' \leq 2)$ population distribution of 1.00 : 0.29 : 0.11 for $v' = 0, 1$ and 2, respectively, we measure a ratio of (1.52 ± 0.21) (1σ). This represents an increase in the $[\text{NO}(B^2\Pi_r, v'=0)]$ of a factor of ~ 5 relative to the $[\text{NO}(A^2\Pi^+, v'=0)]$. We also determined the

ratio $\frac{\gamma_1}{\beta_0}$ using the 1,8 transition of the $\text{NO}(A^2\Sigma^+, v' \rightarrow X^2\Pi_r, v'')$ γ bands and the 0,7 transition

of the $\text{NO}(B^2\Pi_r, v' \rightarrow X^2\Pi_r, v'')$ β bands. While the rate of increase for the production of the γ_1 relative to the β_0 is nearly identical to that observed for the production of the γ_0 relative to the β_0 band, the ratio of γ_1 to β_0 is much smaller (see Table 2).

A very small enhancement in the emission from the $\text{NO}(B^2\Pi_r, v' \rightarrow X^2\Pi_r, v'')$ β bands is observed when the vibrational level population distribution of the $\text{N}_2(A^3\Sigma_u^+)$ state is shifted to higher vibrational levels in the observation region of the rapidly pumped discharge-flow reactor, i.e., $0 \leq v' \leq 6$ (see Figure 8-4). A probable reason for this small increase is that previous work²⁵ has shown that the $[\text{N}_2(A^3\Sigma_u^+, v' \geq 3)]$ decreases by a factor of ~ 2.5 for each vibrational level relative to the $v-1$ level. We know that the $[\text{N}_2(A^3\Sigma_u^+, v' \geq 3)] < [\text{N}_2(A^3\Sigma_u^+, v' \leq 2)]$ ^{25,33}. The concentration of these vibrational levels will be further attenuated when $\text{NO}(X^2\Pi_r)$ is added to the flow. It is possible that we have attenuated the concentrations of the higher vibrational levels to concentrations below which we will see a significant effect on the product emissions. An efficient and clean technique to generate $\text{N}_2(A^3\Sigma_u^+, v' \geq 3)$ in substantial quantities would enable the further investigation of the increase in the emissions from the $\text{NO}(B^2\Pi_r, v' \rightarrow X^2\Pi_r, v'')$ β bands. In addition, the $\text{N}_2(A^3\Sigma_u^+, v' \geq 3)$ Franck-Condon favored^{6,44} $\text{N}_2(A^3\Sigma_u^+, v' \rightarrow X^1\Sigma_g^+, v'')$ Vegard-Kaplan transitions possess enough energy⁴³ to dissociate $\text{NO}(X^2\Pi_r)$. As suggested by Golde and Moyle⁴⁸, it is possible that an alternate product channel is accessible to the $\text{N}_2(A^3\Sigma_u^+, v' \geq 3)$.

Emission from the $2, v''$ transition of the $\text{NO}(A^2\Sigma^+, v' \rightarrow X^2\Pi_r, v'')$ γ bands could be a potential source of interference in the present investigation. In the wavelength region that we made our measurements, the $0,7$ transition of the $\text{NO}(B^2\Pi_r, v' \rightarrow X^2\Pi_r, v'')$ β bands and the $0,8$ transition of the $\text{NO}(B^2\Pi_r, v' \rightarrow X^2\Pi_r, v'')$ β bands are overlapped by the $2,9$ and $2,10$ transitions of the $\text{NO}(A^2\Sigma^+, v' \rightarrow X^2\Pi_r, v'')$ γ bands, respectively. We see a small emission to the blue of the $0,7$ transition of the $\text{NO}(B^2\Pi_r, v' \rightarrow X^2\Pi_r, v'')$ β bands, which might be from the $2,9$ transition of the $\text{NO}(A^2\Sigma^+, v' \rightarrow X^2\Pi_r, v'')$ γ bands. In both cases, the majority of the emission from the $2, v''$ transition of the $\text{NO}(A^2\Sigma^+, v' \rightarrow X^2\Pi_r, v'')$ γ bands is to the blue of the respective $0, v''$ transition of the $\text{NO}(B^2\Pi_r, v' \rightarrow X^2\Pi_r, v'')$ β bands. The Franck-Condon factors^{44,45} for the $2,9$ and $2,10$ transitions of the $\text{NO}(A^2\Sigma^+, v' \rightarrow X^2\Pi_r, v'')$ γ bands are relatively small, i.e., 0.062 and 0.038 ,

respectively. We know that the ratio $\frac{[\text{NO}(A, v' = 2)]}{[\text{NO}(A, v' = 0)]}$ is $\leq 2\%$ of the total $\text{NO}(A \ ^2\Sigma^+, v')$ ⁴⁸. The

error introduced by this weak overlapping emission is therefore small compared to our total reported uncertainty.

The increase in the $[\text{NO}(B \ ^2\Pi_r)]$ with vibrational quanta in the $\text{N}_2(A \ ^3\Sigma_u^+)$ is probably due to a combination of energetics and Franck-Condon overlap ²⁰. We are currently investigating the effect of vibrational energy in the $\text{CO}(a \ ^3\Pi, v')$ on the products of the energy transfer reaction $\text{CO}(a \ ^3\Pi, v') + \text{NO}(X \ ^2\Pi_r, v'')$. A comparison of the product distributions for these two systems might provide some insight into the mechanisms for the excitation of the $\text{NO}(A \ ^2\Sigma^+)$ and $\text{NO}(B \ ^2\Pi_r)$ states.

3.2 BRANCHING FRACTIONS OF THE PRODUCT $\text{NO}(A \ ^2\Sigma^+, v' = 0, 1 \text{ AND } 2)$ AND $\text{NO}(B \ ^2\Pi_r, v' = 0)$ EMISSIONS OBSERVED AS A FUNCTION OF v' IN THE ENERGY TRANSFER REACTION $\text{CO}(a \ ^3\Pi, v') + \text{NO}(X \ ^2\Pi_r, v'' = 0)$

3.2.1 Analysis of the $\text{NO}(A \ ^2\Sigma^+, v')$ and $\text{NO}(B \ ^2\Pi_r, v')$ Emissions.

A series of product photoelectric emission spectra is presented in Figure 9 for the energy transfer reaction $\text{CO}(a \ ^3\Pi, v') + \text{NO}(X \ ^2\Pi_r)$. We show emission spectra for three of the four generating reactions used. From bottom to top they are: (A) $\text{Ar}(^3P_{2,0}) + \text{CO}_2(X \ ^1\Sigma_g^+)$, (B) $\text{He}(^3S_1) + \text{CO}_2(X \ ^1\Sigma_g^+)/\text{CO}(X \ ^1\Sigma^+)/\text{SF}_6$ and (C) $\text{He}(^3S_1) + \text{CO}_2(X \ ^1\Sigma_g^+)/\text{SF}_6$. Each generating reaction provides us with a different $\text{CO}(a \ ^3\Pi)$ vibrational level population distribution at the observation region of the rapidly pumped discharge-flow reactor (See Table 1). Visual comparison of the 0,6 transition of the $\text{NO}(A \ ^2\Sigma^+, v' \rightarrow X \ ^2\Pi_r, v'')$ γ bands at $\sim 2,996 \text{ \AA}$ and the 0,7 transition of the $\text{NO}(B \ ^2\Pi_r, v' \rightarrow X \ ^2\Pi_r, v'')$ β bands at $\sim 3,035 \text{ \AA}$ shows a marked increase in the intensity of the $\text{NO}(B \ ^2\Pi_r, v' \rightarrow X \ ^2\Pi_r, v'')$ β bands relative to the $\text{NO}(A \ ^2\Sigma^+, v' \rightarrow X \ ^2\Pi_r, v'')$ γ bands as $\text{CO}(a \ ^3\Pi)$ increases its $v' > 0$ population in the observation region.

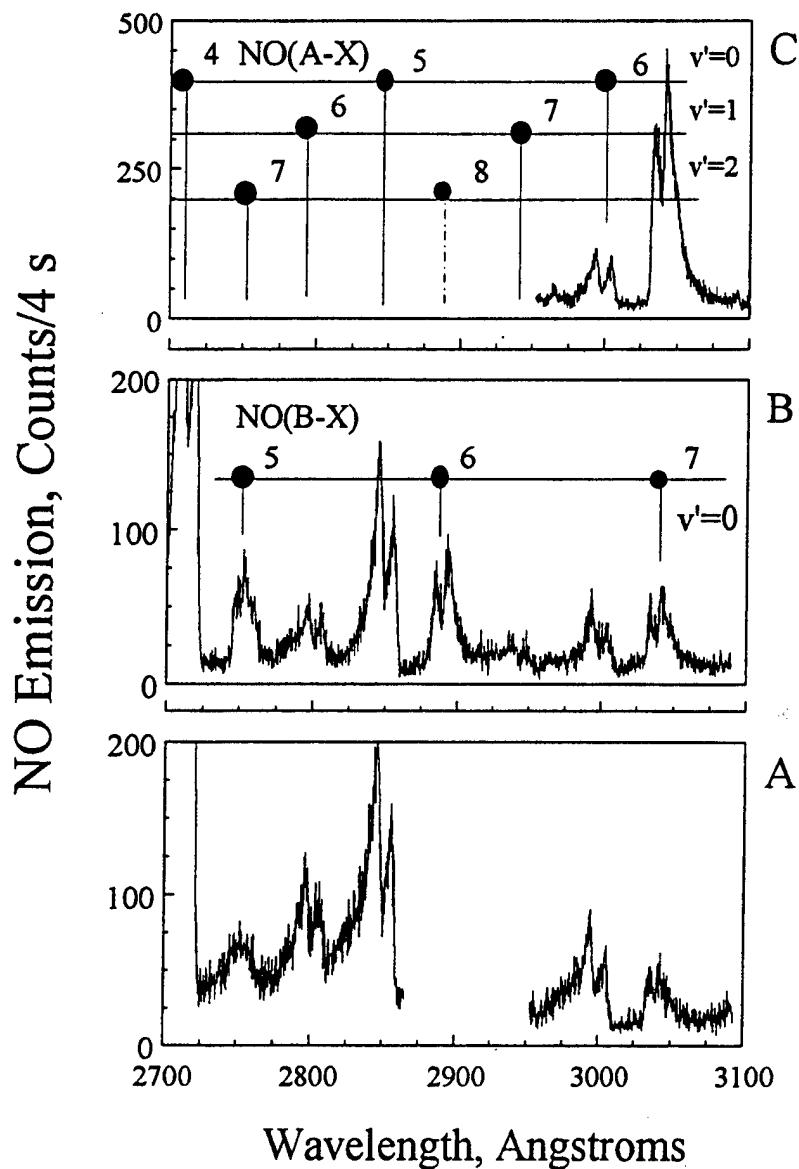


Figure 9. Photoelectric emission spectra for the energy transfer reaction
 $\text{CO}(a, v') + \text{NO}(X, v''=0) \rightarrow \text{CO}(X, v'') + \text{NO}(A, v') + \text{NO}(B, v')$.
 See text for discussion.

The relative populations of the $\text{CO}(a^3\Pi, v')$, $\text{NO}(A^2\Sigma^+, v')$ and $\text{NO}(B^2\Pi_r, v')$ are calculated using the standard equation for emission intensity⁴⁰. The emission intensity, $I_{v', v''}$, for a transition from v' to v'' is given by

$$I_{v', v''} = \kappa \cdot N_{v'} \cdot q_{v', v''} \cdot v_{v', v''}^3 \cdot R_c^2(r_{v', v''}) \cdot R_{v', v''} \quad (5)$$

where κ is a constant, $N_{v'}$ is the number density for molecules in the v' level in cm^{-3} , $q_{v',v''}$ is the Franck-Condon factor for the $v'-v''$ transition, $v_{v',v''}$ is the energy in wavenumber for the $v'-v''$ transition ⁴³, $R_e(r_{v',v''})$ is the electronic transition moment, $r_{v',v''}$ is the r -centroid for the $v'-v''$ transition, and $R_{v',v''}$ is the factor that accounts for the sensitivity of the detection system at the $v'-v''$ transition. The Franck-Condon factors and the r -centroids for the $\text{CO}(a^3\Pi \rightarrow X^1\Sigma^+)$ Cameron bands, $\text{NO}(A^2\Sigma^+,v' \rightarrow X^2\Pi_r,v'')$ γ bands and $\text{NO}(B^2\Pi_r,v' \rightarrow X^2\Pi_r,v'')$ β bands are calculated using a technique described by Rabalais ⁴⁴ and they are found to be in very good agreement with those reported by Krupenie ⁴⁹ for the $\text{CO}(a^3\Pi \rightarrow X^1\Sigma^+)$ Cameron bands and with those reported by Piper and Cowles ⁴⁵ for the $\text{NO}(A^2\Sigma^+,v' \rightarrow X^2\Pi_r,v'')$ γ bands and $\text{NO}(B^2\Pi_r,v' \rightarrow X^2\Pi_r,v'')$ β bands. $R_e(r_{v',v''})$'s for the $\text{NO}(A^2\Sigma^+,v' \rightarrow X^2\Pi_r,v'')$ γ bands are calculated using an expression reported by Piper and Cowles ⁴⁵,

$$R_e(r_{v',v''}) = 33.08 - 58.77 \cdot r_{v',v''} + 26.85 \cdot r_{v',v''}^2 \quad (6)$$

$R_e(r_{v',v''})$'s for the $\text{NO}(B^2\Pi_r,v' \rightarrow X^2\Pi_r,v'')$ β bands are calculated using an expression reported by Piper *et al.* ⁴⁶,

$$R_e(r_{v',v''}) = 0.350 - 0.104 \cdot r_{v',v''} + 3.69 \times 10^4 \cdot e^{-(10.1 \cdot r_{v',v''})} \quad (7)$$

$R_{v',v''}$ is determined using a technique described by Mumma and Zipf ³⁴. $N_{v'}$ is determined by rearranging Eq (5) and κ will be canceled in the determination of the ratios for $N_{v'}$,

$$N_{v'} = \frac{I_{v',v''}}{q_{v',v''} \cdot v_{v',v''}^3 \cdot R_e^2(r_{v',v''}) \cdot R_{v',v''} \cdot \kappa} \quad (8)$$

The emission intensity is calculated numerically by integrating the observed emission spectrum, *i.e.*, $I_{v',v''} = \sum_i I_i \delta E_i$, where δE_i is determined using $\frac{E_{i-1} + E_{i+1}}{2}$. The observed wavelengths are converted to energies using a technique described by Srinivas and Lakshman ⁴⁷.

A summary of the $\text{NO}(A\ 2\Sigma^+, v' \leq 2)$ and $\text{NO}(B\ 2\Pi_r, v'=0)$ population distributions and branching fractions are presented in Table 3 for the four different $\text{CO}(a\ 3\Pi, v')$ vibrational distributions used (See Table 1). The relative $\text{NO}(A\ 2\Sigma^+, v' \leq 2)$ and $\text{NO}(B\ 2\Pi_r, v'=0)$ populations are calculated using Eq (8). Band intensities from the $\text{NO}(A\ 2\Sigma^+, v'=0-2 \rightarrow X\ 2\Pi_r, v'')$ γ , $\Delta v = v' - v'' = -4, -5$ and -6 and the $\text{NO}(B\ 2\Pi_r, v'=0 \rightarrow X\ 2\Pi_r, v'')$ β , $\Delta v = -6$ and -7 bands were used to determine the $N_{v'}$'s for the $\text{NO}(A\ 2\Sigma^+, v'=0, 1$ and $2)$ and the $\text{NO}(B\ 2\Pi_r, v'=0)$. The branching fractions were then determined for each of the observed emissions in a given measurement where

$$\sum_{v'=0}^{v'_{\max}} N_{v'} = \sum_{v'=0}^{v'_{\max}} N_{A,v'} + \sum_{v'=0}^{v'_{\max}} N_{B,v'} = 1, \text{ where } v'_{\max} \text{ is } 2 \text{ and } 0 \text{ for the } \text{NO}(A\ 2\Sigma^+) \text{ and } \text{NO}(B\ 2\Pi_r)$$

states, respectively. Immediately obvious in Table 3 is the large increase in the production of $\text{NO}(B\ 2\Pi_r, v'=0)$ relative to $\text{NO}(A\ 2\Sigma^+, v'=0)$ as the higher vibrational levels of the $\text{CO}(a\ 3\Pi)$ are populated in the observation region (See Table 2). The ratio $\frac{\gamma_0}{\beta_0}$, where the subscript 0 refers to

their respective $N_{v'=0}$ value Eq (8), is determined to be (0.65 ± 0.02) (1σ) for the energy transfer reaction $\text{CO}(a\ 3\Pi, v'=0) + \text{NO}(X\ 2\Pi_r, v''=0)$. As the vibrational level population distribution in the $\text{CO}(a\ 3\Pi)$ is shifted to higher vibrational levels, we see an increase in the intensity of the $\text{NO}(B\ 2\Pi_r, v'=0 \rightarrow X\ 2\Pi_r, v'')$ β bands relative to the $\text{NO}(A\ 2\Sigma^+, v' \rightarrow X\ 2\Pi_r, v'')$ γ bands. For the energy transfer reaction $\text{He}(3S_1) + \text{CO}_2(X\ 1\Sigma_g^+)$, which represents the most unrelaxed $\text{CO}(a\ 3\Pi)$

vibrational level population distribution used in the present investigation, we see the ratio $\frac{\gamma_0}{\beta_0}$

decrease to a value of (0.099 ± 0.004) (1σ). This represents a factor of (6.6 ± 0.3) (1σ) increase in the $[\text{NO}(B\ 2\Pi_r, v'=0)]$ relative to the $[\text{NO}(A\ 2\Sigma^+, v'=0)]$.

Table 3: Relative populations and branching fractions for the NO(A,B) states.^a

Generating Reaction ^b	NO(A $^2\Sigma^+, v'$)			NO(B $^2\Pi_r, v''=0$)	$\frac{[\text{NO}(A, v'=0)]}{[\text{NO}(A, v'=1)]}$ ^c
	$v' = 0$	$v' = 1$	$v' = 2$		
Ar* + CO ₂	0.355 ± 0.009	0.081 ± 0.030	0.017 ± 0.003	0.546 ± 0.013	0.650 ± 0.022
Ar* + CO/CO ₂	0.382 ± 0.031	0.055 ± 0.005	d	0.563 ± 0.045	0.679 ± 0.077
He* + CO/CO ₂ /SF ₆	0.166 ± 0.013	0.020 ± 0.003	d	0.815 ± 0.199	0.204 ± 0.033
He* + CO ₂ /SF ₆	0.088 ± 0.002	0.013 ± 0.001	0.012 ± 0.001	0.888 ± 0.025	0.099 ± 0.004

a) The relative intensities were calculated using Equation 4 and emission from the NO γ $v' = 0-2$ $\Delta v = v' - v'' = -4, -5$ and -6 bands and the NO β $v' = 0$ $\Delta v = -6$ and -7 bands. The uncertainties reported in the table account for the statistical uncertainty (1s) associated with the measurements. An additional 12% should be added in quadrature to the above uncertainties to account for the total experimental uncertainty.

b) Ar or He metastables were generated using a low power dc discharge in Ar or He. See Table 1 for the CO($a^3\Pi, v$) vibrational distribution that corresponds to each of these generating reactions.

c) The ratio, $\gamma_0/\beta_0 = N_{A, v'=0}/N_{B, v''=0}$, is calculated using the standard equation for emission intensity. See text for discussion.

d) In the experiments in which we used a 1:1 mixture of CO₂($X^1\Sigma_g^+$) and CO($X^1\Sigma^+$) to generate the CO($a^3\Pi, v'$) no analysis was performed on the NO(A $^2\Sigma^+, v'=2$) because of a weak signal-to-background-noise in the region we scanned.

As mentioned above, previous work ¹⁷ has attributed the difference in the ratios between the He and Ar systems to trace concentrations of N₂(A $^3\Sigma_u^+$) which results from N₂ impurities in the Ar buffer gas and not to a dependence upon the vibrational level distribution of the CO($a^3\Pi$). Our

results show clearly that N₂ impurities are insignificant in our experiments. The $\frac{\gamma_0}{\beta_0}$ ratios for

the energy transfer reactions CO($a^3\Pi, v'=0,1$) + NO($X^2\Pi_r, v''=0$) and N₂(A $^3\Sigma_u^+, v'=0$) + NO($X^2\Pi_r, v''=0$) are (0.65 ± 0.02) (1 σ) and (7.67 ± 1.16) (1 σ) ⁵⁰, respectively. This large difference in the ratios makes it unlikely that nitrogen is a relevant impurity. We performed a second set of measurements on the energy transfer reaction CO($a^3\Pi, v'=0,1$) + NO($X^2\Pi_r$) using the generating reaction Ar($3P_{2,0}$) + CO₂($X^1\Sigma_g^+$). The [NO($X^2\Pi_r$)] was reduced by a factor of ~10 as compared to that used for the same reaction presented in Table 3. The results of these measurements are given in Table 4. Since the k_v 's for the reactions CO($a^3\Pi$) + NO($X^2\Pi_r$) ¹⁴⁻¹⁷ and N₂(A $^3\Sigma_u^+$) +

$\text{NO}(X^2\Pi_r)$ 3,20 differ by a factor of ~ 4.8 , *i.e.*, $\frac{k_{\text{CO}(a, v'=0)+\text{NO}(X)}}{k_{\text{N}_2(A, v'=0)+\text{NO}(X)}} = \left(\frac{2.9 \cdot 10^{-10}}{6.0 \cdot 10^{-11}} \right) \sim 4.8$, reducing the

$[\text{NO}(X^2\Pi_r)]$ by a factor of ~ 10 will increase the $[\text{CO}(a^3\Pi)]$ relative to the $[\text{N}_2(A^3\Sigma_u^+)]$ in the observation region of the rapidly pumped discharge-flow reactor. If the $\text{CO}(a^3\Pi, v'=0,1)$ are the predominant energy transfer precursors, as we expect them to be, the increase in the relative concentrations of the $\text{CO}(a^3\Pi, v'=0,1)$ corresponding to the factor of 10 decrease in the

$[\text{NO}(X^2\Pi_r)]$ should not change the observed ratio $\frac{\gamma_0}{\beta_0}$ by a significant amount and we might see a

small decrease in the ratio $\frac{\gamma_0}{\beta_0}$. However, if the observed ratio $\frac{\gamma_0}{\beta_0}$ contains a significant

contribution from the energy transfer reaction $\text{N}_2(A^3\Sigma_u^+, v'=0) + \text{NO}(X^2\Pi_r, v''=0)$, *i.e.*,

$\left(\frac{\gamma_0}{\beta_0} \right)_{\text{Observed}} = \frac{\gamma_{0,\text{CO}(a)} + \gamma_{0,\text{N}_2(A)}}{\beta_{0,\text{CO}(a)} + \beta_{0,\text{N}_2(A)}}$, we would expect the observed ratio $\frac{\gamma_0}{\beta_0}$ to increase by a

significant amount. The measured ratio $\frac{\gamma_0}{\beta_0}$ is observed to decrease slightly from (0.65 ± 0.02)

(1σ) to (0.52 ± 0.12) (1σ) when the $[\text{NO}(X^2\Pi_r)]$ is reduced by a factor of ~ 10 . The larger uncertainty associated with the latter measurement is due to the poorer signal-to-noise obtained

when we lowered the $[\text{NO}(X^2\Pi_r)]$. The decrease in the ratio $\frac{\gamma_0}{\beta_0}$, *i.e.*, the increase in the

$[\text{NO}(B^2\Pi_r, v'=0)]$, is due to a small increase in the $[\text{CO}(a^3\Pi, v'=1)]$. We conclude, therefore, that

N_2 is negligible as an impurity and the observed change in the ratio $\frac{\gamma_0}{\beta_0}$ is due to vibrational

energy in the $\text{CO}(a^3\Pi)$ state.

Table 4: Relative populations and branching fractions for the NO(A,B) states as a function of [NO(X)] in the energy transfer reaction CO(a,v'=0) + NO(X,v''=0).

Generating Reaction ^b	NO(A 2Σ ⁺ ,v')			NO(B 2Π _r ,v'=0)	$\frac{[\text{NO}(A,v'=0)]}{[\text{NO}(A,v'=0)]}$ ^c
	v' = 0	v' = 1	v' = 2		
Ar* + CO ₂ ^d	0.355 ± 0.009	0.081 ± 0.030	0.017 ± 0.003	0.546 ± 0.013	0.650 ± 0.022
Ar* + CO ₂ ^e	0.316 ± 0.050	0.061 ± 0.011	0.020 ± 0.003	0.603 ± 0.096	0.524 ± 0.118

a) The relative intensities were calculated using Equation 4 and emission from the NO γ v' = 0-2 Δv = v' - v'' = -4, -5 and -6 bands and the NO β v' = 0 Δv = -6 and -7 bands. The uncertainties reported in the table account for the statistical uncertainty (1σ) associated with the measurements. An additional 12% should be added in quadrature to the above uncertainties to account for the total experimental uncertainty.

b) Ar or He metastables were generated using a low power dc discharge in Ar or He. The CO(a) is primarily in v'=0.

c) The ratio, $\gamma_0/\beta_0 = N_{A,v'=0}/N_{B,v'=0}$, is calculated using the standard equation for for emission intensity. See text for discussion.

d) Data from Table 3. [NO(X)] = (3.78 ± 0.33) x 10¹² molecules cm⁻³.

e) [NO(X)] = (2.24 ± 0.24) x 10¹¹ molecules cm⁻³.

3.2.2 Comparison between the N₂(A 3Σ_u⁺) and CO(a 3Π)

As expected^{17,39}, excitation of the NO(B 2Π_r,v' → X 2Π_r,v'') β bands relative to the NO(A 2Σ⁺,v' → X 2Π_r,v'') γ bands is more efficient for the energy transfer reaction CO(a 3Π,v'=0) + NO(X

2Π_r) as compared to the energy transfer reaction N₂(A 3Σ_u⁺,v'=0) + NO(X 2Π_r), i.e., $\frac{\gamma_0}{\beta_0} = (0.650$

± 0.022) (1σ) and (7.67 ± 1.16) (1σ)⁵⁰, respectively. Using these ratios and normalizing the

CO(a 3Π,v'=0) + NO(X 2Π_r,v'') data to the N₂(A 3Σ_u⁺,v'=0) + NO(X 2Π_r,v'') data, we determine

that the energy transfer reaction CO(a 3Π,v'=0) + NO(X 2Π_r,v''=0) is (21.6 ± 3.3) (1σ) times

more efficient at generating NO(B 2Π_r,v'=0) than the energy transfer reaction N₂(A 3Σ_u⁺,v'=0) +

NO(X 2Π_r,v''=0). This is qualitatively consistent with the work reported by Taylor and

Setser^{17,39}. This observation is even more pronounced when we consider the fact that only

~1/3¹⁴ of the energy transfer reaction CO(a 3Π) + NO(X 2Π_r) leads to the excitation of the NO(A

2Σ⁺) and NO(B 2Π_r) compared to the energy transfer reaction N₂(A 3Σ_u⁺) + NO(X 2Π_r) which is

100% efficient in producing the NO(A 2Σ⁺) and NO(B 2Π_r)^{3,48}.

For the unrelaxed energy transfer reactions $\text{CO}(a^3\Pi, v' \leq 3) + \text{NO}(X^2\Pi_r)$ and $\text{N}_2(A^3\Sigma_u^+, v' \leq 2) +$

$\text{NO}(X^2\Pi_r)$ we measured $\frac{\gamma_0}{\beta_0}$ ratios of (0.099 ± 0.004) (1σ) and (1.54 ± 0.10) (1σ)⁵⁰,

respectively. This represents a factor of approximately 6.5 increase in the $[\text{NO}(B^2\Pi_r, v'=0)]$ relative to the $[\text{NO}(A^2\Sigma^+, v'=0)]$ for the energy transfer reaction $\text{CO}(a^3\Pi, v' \leq 3) + \text{NO}(X^2\Pi_r)$ while the $[\text{NO}(B^2\Pi_r, v'=0)]$ increases by a factor of approximately 5.0 relative to the $[\text{NO}(A^2\Sigma^+, v'=0)]$ for the energy transfer reaction $\text{N}_2(A^3\Sigma_u^+, v' \leq 2) + \text{NO}(X^2\Pi_r)$.

3.3 AN UPPER LIMIT ON THE FORMATION OF $\text{NO}(X^2\Pi_r)$ IN THE REACTIONS $\text{N}_2(A^3\Sigma_u^+) + \text{O}(^3\text{P})$ AND $\text{N}_2(A^3\Sigma_u^+) + \text{O}_2(X^3\Sigma_g^-)$ AT 298 K.

The primary objective of this investigation was to quantify the $\text{NO}(X^2\Pi_r) + \text{N}(^4\text{S}, ^2\text{D})$ product yield from the reaction $\text{N}_2(A^3\Sigma_u^+) + \text{O}(^3\text{P})$. For the reaction $\text{N}_2(A^3\Sigma_u^+, v' \leq 2) + \text{O}(^3\text{P})$ there is no $[\text{NO}(X^2\Pi_r)]_{\text{Observed}}$ detected above the noise in the background emission signal. After correcting this null measurement for competing $\text{N}_2(A^3\Sigma_u^+)$ removal processes the upper limit for the corrected $\text{NO}(X^2\Pi_r) + \text{N}(^4\text{S}, ^2\text{D})$ product yield, $[\text{NO}(X^2\Pi_r)]_{\text{Product}}$, in the reaction $\text{N}_2(A^3\Sigma_u^+, v' \leq 2) + \text{O}(^3\text{P})$ is $[\text{NO}(X^2\Pi_r)]_{\text{Product}} = \frac{[\text{NO}(X^2\Pi_r)]_{\text{Observed}}}{F_{\text{O}(^3\text{P})}} \leq 2\%$ (Signal-to-Background

Noise=1, 1σ) of the $[\text{N}_2(A^3\Sigma_u^+, v' \leq 2)]_{\text{Total}}$. When the $\text{N}_2(A^3\Sigma_u^+, v')$ population is shifted to higher vibrational levels, i.e., $0 \leq v' \leq 6$, by reducing the $[\text{N}_2]_{\text{Total}}$ from $\sim 20\%$ to $\sim 0.2\%$ of the total flow a small increase in the $[\text{NO}(X^2\Pi_r)]_{\text{Observed}}$ was detected above the noise in the background. After correcting the $[\text{NO}(X^2\Pi_r)]_{\text{Observed}}$ for competing $\text{N}_2(A^3\Sigma_u^+, v' \leq 6)$ loss processes the $[\text{NO}(X^2\Pi_r)]_{\text{Product}}$ accounts for $\sim 5.7\%$ of the $[\text{N}_2(A^3\Sigma_u^+, v' \leq 6)]_{\text{Total}}$. This product emission was attenuated by the addition of CH_4 to the flow upstream of the reaction zone suggesting that the emission signal is due to the presence of $\text{N}_2(A^3\Sigma_u^+, v' \geq 3)$.

For the low-[N₂] experiments the corrected NO(*X*²Π_r) + N(4S,2D) product yield represents (5.7 ± 1.1)% (1σ) of the [N₂(*A*³Σ_u⁺)]_{Total}. If the NO(*X*²Π_r) is indeed formed by reaction of higher vibrational levels of the N₂(*A*³Σ_u⁺) the vibrational level specific branching fraction is probably much higher since the relative population of N₂(*A*³Σ_u⁺, *v*' ≥ 3) is significantly smaller than the lower vibrational levels. Based on laser-excited fluorescence measurements^{25,33} and vibrational relaxation studies^{22,25}, we estimate that the fractional N₂(*A*³Σ_u⁺) population in *v*' ≥ 3 is <10% of the total N₂(*A*³Σ_u⁺), which suggests that the NO(*X*²Π_r) + N(4S,2D) product yield could be ≥(57 ± 14)% of the total [N₂(*A*³Σ_u⁺, *v*' ≥ 3)].

As mentioned above, the reactions N₂(*A*³Σ_u⁺) + O₂(*X*³Σ_g⁻) and N₂(*A*³Σ_u⁺) + O₂* could interfere with the measurement of the NO(*X*²Π_r) + N(4S,2D) product channel in the reaction N₂(*A*³Σ_u⁺) + O(³P). The product channels for the reaction N₂(*A*³Σ_u⁺) + O₂(*X*³Σ_g⁻) have been extensively studied⁵¹⁻⁵⁵; however, previous studies did not look at the formation of NO(*X*²Π_r). Although the NO(*X*²Π_r) + NO(*X*²Π_r) product channel is 4.3 eV exoergic the probability of the *four-centre* chemical reaction is very small⁵⁶. No [NO(*X*²Π_r)]_{Observed} is detected above the noise in the background emission signal from the reaction N₂(*A*³Σ_u⁺) + O₂(*X*³Σ_g⁻, *v*" = 0). With a detection limit of ~2 × 10⁷ molecules cm⁻³ (Signal-to-Background Noise = 1, 1σ) this represents a corrected

branching fraction
$$[\text{NO}(X^2\Pi)]_{\text{Product}} = \frac{[\text{NO}(X^2\Pi)]_{\text{Observed}}}{F_{\text{O}_2}}$$
 of < 0.1% of the [N₂(*A*³Σ_u⁺)]_{Total}.

This measurement was insensitive to the N₂(*A*³Σ_u⁺) vibrational level population distribution for *v*' ≤ 6 and showed that the presence of undissociated O₂(*X*³Σ_g⁻) would not interfere with the N₂(*A*³Σ_u⁺) + O(³P) → NO(*X*²Π_r) + N(4S,2D) product channel measurement. The product channels for the reaction of N₂(*A*³Σ_u⁺) + O₂* are not well characterized. The effect of this reaction on the present analysis will be discussed below.

Several key assumptions were made in the data analysis and interpretation. First, we assume that the initial concentration of the $N_2(A\ ^3\Sigma_u^+)$, $[N_2(A\ ^3\Sigma_u^+)]_{\text{Initial}}$, is equal to the concentration of the Xe metastables, $Xe(3P_{2,0})$, at the N_2 inlet. Work by Sadeghi and Setser⁵⁷ has shown that the primary product in the energy transfer reaction $Xe(3P_{2,0}) + N_2(X\ ^1\Sigma_g^+)$ is $N_2(B\ ^3\Pi_g)$. $N_2(A\ ^3\Sigma_u^+)$ is then formed in the subsequent rapid collisional and radiative cascade in the triplet manifold of electronically excited N_2 .

Second, we assume that $[Xe(3P_{2,0})] = [O(^3P)]/2$ at the N_2 inlet. Balamuta and Golde^{58,59} have determined that the reaction $Xe(3P_{2,0}) + O_2$ produces two atomic oxygen for each Xe metastable. Although this reaction is sufficiently exoergic to generate $O(^1D)$, under our experimental conditions any $O(^1D)$ formed in the titration reaction would be rapidly quenched by the excess O_2 and Ar⁶⁰. The loss of $O(^3P)$ at the walls of the reactor is small and is therefore neglected ($k_{\text{WALL,PYREX}} \sim 2\ \text{s}^{-1}$)⁶¹.

Third, we assume that the only loss process for $N_2(A\ ^3\Sigma_u^+)$ in the short time from the N_2 inlet to the $O(^3P)/O_2$ addition port ($t \sim 2\ \text{ms}$), is the deactivation of $N_2(A\ ^3\Sigma_u^+)$ at the wall^{37,62}, $k_{\text{WALL}} \sim 176\ \text{s}^{-1}$. This is reasonable since both Ar and N_2 are known to be very inefficient electronic quenchers of the $N_2(A\ ^3\Sigma_u^+)$ ^{9,11,63}.

Fourth, the $[NO(X\ ^2\Pi_r)]_{\text{Observed}}$ is not affected by the $N_2(A\ ^3\Sigma_u^+)$ radial concentration gradient which results from the deactivation of $N_2(A\ ^3\Sigma_u^+)$ at the reactor walls⁶⁴. Iannuzzi *et al.*⁵¹ investigated this problem while determining the $N_2O + O$ branching fraction in the reaction $N_2(A\ ^3\Sigma_u^+) + O_2(X\ ^3\Sigma_g^-)$. It was determined that the $[N_2(A\ ^3\Sigma_u^+)]$ gradient had <10% effect on their product channel measurement. The effect of a concentration gradient in the present investigation would be of the same magnitude determined by Iannuzzi *et al.*⁵¹ since our measurements were performed under similar flow conditions.

Fifth, if the $\text{NO}(X^2\Pi_r)$ formed in the reaction $\text{N}_2(A^3\Sigma_u^+) + \text{O}(^3\text{P})$ is vibrationally hot, i.e., $v'' \leq 14$ and $v'' \leq 6$ for processes (3) and (5) in Table 5, respectively, it will be vibrationally relaxed into $v''=0$ within the ~ 40 cm (10 ms) reaction distance. $\text{O}(^3\text{P})$ is a very efficient vibrational relaxant of $\text{NO}(X^2\Pi_r, v'')$. For $\text{NO}(X^2\Pi_r, v''=1) + \text{O}(^3\text{P}) \rightarrow \text{NO}(X^2\Pi_r, v''=0) + \text{O}(^3\text{P})$ Fernando and Smith⁶⁵ report a $k = 6.5 \times 10^{-11} \text{ cm}^3 \text{ molecules}^{-1} \text{ s}^{-1}$. If k is similarly large for higher v'' , as it is expected to be, $>95\%$ of the product $\text{NO}(X, v'' \geq 1)$ should be relaxed into $v''=0$ prior to the NO laser-excited fluorescence detector port. This lower limit is based on a set of Runge-Kutta fourth order numerical calculations with automatic step sizing that used as input parameters the rate constant reported by Fernando and Smith⁶⁵ for the $\text{NO}(X^2\Pi_r, v'') + \text{O}(^3\text{P}) \rightarrow \text{NO}(X^2\Pi_r, v''-1) + \text{O}(^3\text{P})$, a worst case scenario where all the product $\text{NO}(X^2\Pi_r)$ is initially populated in $v''=14$ and concentrations and residence times associated with the respective measurements. In addition, further vibrational relaxation of the $\text{NO}(X^2\Pi_r, v'' \geq 1)$ would have been observed in the measurements where we vibrationally relaxed $\text{N}_2(A^3\Sigma_u^+, v' \geq 1)$ into $\text{N}_2(A^3\Sigma_u^+, v'=0)$ using CH_4 . CH_4 , while not as efficient as $\text{O}(^3\text{P})$, is known to vibrationally relax $\text{NO}(X^2\Pi_r, v''=1)$ with a reported rate constant $k = (1.88 \pm 0.15) \times 10^{-13} \text{ cm}^3 \text{ molecules}^{-1} \text{ s}^{-1}$.⁶⁶

Table 5: Exothermic product channels for the reaction $\text{N}_2(A^3\Sigma_u^+, v'=0) + \text{O}(^3\text{P})$

$\text{N}_2(A^3\Sigma_g^+) + \text{O}(^3\text{P})$	$\rightarrow \text{N}_2(X^1\Sigma_g^+) + \text{O}(^3\text{P}) + 6.2 \text{ eV}$	(1)
	$\rightarrow \text{N}_2(X^1\Sigma_g^+) + \text{O}(^1\text{D}) + 4.2 \text{ eV}$	(2)
	$\rightarrow \text{NO}(X^2\Pi_r) + \text{N}(^4\text{S}) + 2.9 \text{ eV}$	(3)
	$\rightarrow \text{N}_2(X^1\Sigma_g^+) + \text{O}(^1\text{S}) + 2.0 \text{ eV}$	(4)
	$\rightarrow \text{NO}(X^2\Pi_r) + \text{N}(^2\text{D}) + 0.5 \text{ eV}$	(5)

We must also consider the possible interference that would occur if significant quantities of atomic nitrogen are present in the reaction zone. The presence of atomic nitrogen would result in an underestimate of the $\text{NO}(X^2\Pi_r) + \text{N}(^4\text{S}, ^2\text{D})$ and $\text{NO}(X^2\Pi_r) + \text{NO}(X^2\Pi_r)$ product yields since the reaction $\text{N} + \text{NO} \rightarrow \text{N}_2 + \text{O}$ is fast, $k = 3.4 \times 10^{-11} \text{ cm}^3 \text{ molecules}^{-1} \text{ s}^{-1}$ at 298 K⁶⁷. In a separate experiment²⁵, the N_2 flow was replaced by a comparable flow of Ar and the relative

concentration of the $N_2(A^3\Sigma_u^+, v'=3)$ was monitored by laser-excited fluorescence techniques in order to place an upper limit on the concentration of the atomic nitrogen in the reaction zone. No $N_2(A^3\Sigma_u^+, v'=3)$ laser-excited fluorescence emission signal was observed above the noise in the background. We corrected the null $N_2(A^3\Sigma_u^+, v'=3)$ measurement for the $N_2(A^3\Sigma_u^+, v')$ population distribution^{22,25,33} and wall loss in the reaction zone^{37,62}. Then, assuming a worse case scenario in which all of the N_2 -impurity would be dissociated into atomic nitrogen in the metastable generation region, we estimate an upper limit of $\sim 5 \times 10^9$ molecules cm^{-3} for the atomic nitrogen concentration. Based on this value the subsequent reduction of any NO product formed in the title reactions from the reaction $N + NO$ would amount to less than 0.2% of the total NO.

Several of the interactions can be eliminated as possible sources of $NO(X^2\Pi_r)$. First, the reaction $N_2^* + O_2(X^3\Sigma_g^-)$, where $N_2^* \equiv N_2(A^3\Sigma_u^+)$, $N_2(B^3\Pi_g)$, and $N_2(W^3\Delta_u)$ states, can be eliminated since there is no $[NO(X^2\Pi_r)]_{\text{Observed}}$ detected in the preliminary $N_2(A^3\Sigma_u^+, v') + O_2(X^3\Sigma_g^-)$ measurements and all of the above species would have been present in the reaction zone in either the low- or high- $[N_2]$ experiments. Second, the reaction $N_2(A^3\Sigma_u^+, v' \leq 2) + O_2^*$, where $O_2^* \equiv O_2(a^1\Delta)$ and $O_2(b^1\Sigma_g^+)$, can also be eliminated as a source of $NO(X^2\Pi_r)$ since the O_2^* is present in the high- $[N_2]$ $N_2(A^3\Sigma_u^+, v' \leq 2) + O(^3P)$ experiments. Third, the reaction $N_2(A^3\Sigma_u^+, v' \leq 2) + O(^3P)$ can be eliminated since no $[NO(X^2\Pi_r)]_{\text{Observed}}$ is detected in the present investigation. Fourth, it is unlikely that the reactions $N_2(B^3\Pi_g) + O(^3P)$ or $N_2(W^3\Delta_u) + O(^3P)$ are responsible for the production of $NO(X^2\Pi_r)$ because of their short lifetimes ($\tau \sim 8\mu\text{s}$) and low concentrations in the reaction zone. There remain two possible sources of product $NO(X^2\Pi_r)$: $N_2(A^3\Sigma_u^+, v' \geq 3) + O(^3P)$ and/or $N_2(A^3\Sigma_u^+, v' \geq 3) + O_2^*$. Very little is known about the excited state surfaces of N_2O ⁶⁸. Molecular correlation diagrams for the $O + N_2$ reaction in $C_{\infty v}$, C_{2v} and C_s symmetries have been constructed by Michels⁶⁸.

Without a detailed knowledge of the activation barriers and other surface characteristics, a 50% branching fraction can be estimated for the $\text{NO}(X^2\Pi_r) + \text{N}(4S, 2D)$ product channel in $C_{\infty v}$ symmetry where three of the six surfaces are reactive⁶⁸, *i.e.*, the $1\Sigma^-$, 5Π and the $5\Sigma^-$. In C_{2v} and C_s symmetries only 1/3 of the surfaces are reactive⁶⁸. While the formation of the $\text{NO} + \text{N}(4S, 2D)$ in the reaction $\text{N}_2(A^3\Sigma_u^+) + \text{O}(3P)$ can be explained using correlation diagrams, it appears that the major $\text{N}_2(A^3\Sigma_u^+)$ deactivation process proceeds via a curve crossing mechanism to form $\text{N}_2(X^1\Sigma_u^+) + \text{O}(1S)$ with the direct formation of $\text{NO}(X^2\Pi_r)$ being negligible for $\text{N}_2(A^3\Sigma_u^+)$ in the low vibrational levels, *i.e.*, $v' \leq 2$. The magnitude of the observed increase in the $\text{NO} + \text{N}(4S, 2D)$ branching fraction from $\leq 2\%$ of the $[\text{N}_2(A^3\Sigma_u^+, v' \leq 2)]_{\text{Total}}$ for the reaction $\text{N}_2(A^3\Sigma_u^+, v' \leq 2) + \text{O}(3P)$ to $(57 \pm 14)\%$ of the $[\text{N}_2(A^3\Sigma_u^+, 3 \leq v' \leq 6)]_{\text{Total}}$ for the reaction $\text{N}_2(A^3\Sigma_u^+, v' \geq 3) + \text{O}(3P)$ is consistent with the predictions made using the molecular correlation diagrams; however, it suggests that there is an energy barrier associated with this channel.

3.4 PROGRAM ENHANCEMENTS TO THE $\text{NO}(A^2\Sigma^+, v' \rightarrow X^2\Pi_r, v'')$ γ BANDS SYNTHETIC SPECTRUM GENERATION CODE

The analysis of the rotational structure of the $\text{NO}(A^2\Sigma^+, v' \rightarrow X^2\Pi_r, v'')$ γ bands observed in the energy transfer reaction $\text{N}_2(A^3\Sigma_u^+, v') + \text{NO}(X^2\Pi_r)$ has been described in detail previously²¹.

The original computer code was developed using Microsoft's BASIC Professional Development System v7.x, electronic term energies presented in Huber and Herzberg⁴³ and energy level equations presented in Engleman *et al.*⁶⁹ for the $\text{NO}(A^2\Sigma^+)$ and $\text{NO}(X^2\Pi_r)$ states. Agreement with published line assignments for low N' values is excellent⁶⁹; however, the agreement is not as good for $N' > 15$, *i.e.*, $d\lambda \sim 0.5 \text{ \AA}$ at $N'=25$. Since the calculated line positions for $N' \geq 15$ were only in satisfactory agreement with the observed line positions, the rotational temperature of the $\text{NO}(A^2\Sigma^+)$ state was determined using a Fractional Area Technique²¹. This technique is not sensitive to the absolute location of the line positions and provides a satisfactory method to determine the rotational temperature of the product $\text{NO}(A^2\Sigma^+)$.

To improve the agreement between the observed and calculated line positions the code was modified to use the energy level equations for a $2\Sigma^-2\Pi$ system found in Huber and Herzberg⁴³. Agreement between the calculated and observed wavelengths for the $\text{NO}(A\ 2\Sigma^+,v' \rightarrow X\ 2\Pi_r,v'')$ γ bands in the updated code is excellent for low N' and for high N' the agreement between the calculated and observed line positions was better than that obtained using the Engleman *et al.*⁶⁹ data. Recently, a manuscript published by Amiot *et al.*⁷⁰ was found in the literature. Their work provides better electronic term values for the $\text{NO}(X\ 2\Pi_r)$ state and these values were incorporated into the Synthetic Spectrum Program during the program's conversion from DOS to Windows. The new version of the program was developed using Microsoft's Visual BASIC v3.x Professional Edition. The new term values provide excellent agreement with published line assignments⁶⁹ for both the low and high N' values. A summary of the reported line assignments and the calculated line positions is presented in Tables 6 and 7 for the F_1 and F_2 components of the $\text{NO}(A\ 2\Sigma^+,v' \rightarrow X\ 2\Pi_r,v'')$ $\gamma_{0,0}$ band, respectively. The Engleman *et al.*⁶⁹ data represents the observed line assignments. The difference between the observed and calculated line positions in cm^{-1} is presented in Tables 8 and 9 for the F_1 and F_2 components of the $\text{NO}(A\ 2\Sigma^+,v' \rightarrow X\ 2\Pi_r,v'')$ $\gamma_{0,0}$ band, respectively. For clarity, the difference between the observed and calculated line positions in \AA is presented in Tables 10 and 11 for the F_1 and F_2 components of the $\text{NO}(A\ 2\Sigma^+,v' \rightarrow X\ 2\Pi_r,v'')$ $\gamma_{0,0}$ band, respectively. For this analysis the wavelengths were calculated by simply taking the reciprocal of the calculated energy and multiplying this result by 10^8 . The small vacuum-to-air correction is not applied to these calculations⁴⁷. As seen in Tables 10 and 11 the agreement between the observed and calculated line positions is excellent for low N' , independent of the term energies used and expressions used to calculate the T_{E+V+R} value. For high N' , *i.e.*, $N' > 5$, only the data published by Amiot *et al.*⁷⁰ provides excellent agreement between the observed and calculated line positions. The anomalous deviation in Table 11 for the Amiot *et al.*⁷⁰ data for the dR_2 branch at $N' = 10$ is due to the fact that the reported line is a blend and not a single line assignment. The difference between the Herzberg and Amiot data presented in Tables 6 through 11 is the source of the term energies for the ground state of NO. The energy level equations are the same for both sets of data. In general, the Amiot term energies

provide better than a factor of 10 improvement over the Herzberg term energies in the accuracy of the calculated line positions.

Table 6: Reported and Calculated Energies for the F(1) component of the NO A-X $v'=0, v''=0$ band

N'	P(1), Wavenumbers			Q(1), Wavenumbers			R(1), Wavenumbers			S(21), Wavenumbers		
	Engleman	Herzberg	Amiot	Engleman	Herzberg	Amiot	Engleman	Herzberg	Amiot	Engleman	Herzberg	Amiot
0	44193.94	44194	44193.93	44198.92	44198.99	44198.95						
1	44189.57	44189.66	44189.55	44197.83	44197.97	44197.91	44202.94	44202.96	44202.92			
2	44185.82	44185.96	44185.79	44197.46	44197.61	44197.49	44205.88	44205.92	44205.85	44210.76	44210.91	44210.87
3	44182.66	44182.91	44182.66	44197.69	44197.88	44197.71	44209.43	44209.53	44209.41	44217.88	44217.84	44217.78
4	44180.21	44180.51	44180.16	44198.5	44197.81	44198.55	44213.62	44213.78	44213.6	44225.28	44225.42	44225.31
5	44178.32	44178.75	44178.29	44199.96	44200.38	44200.03	44218.44	44218.67	44218.42	44233.42	44233.64	44233.47
10	44178.32	44179.63	44178.33	44216.67	44217.89	44216.79	44251.92	44252.82	44251.9	44283.57	44284.42	44283.67
15	44193.94	44196.52	44193.97	44248.91	44251.41	44249.14	44300.91	44302.96	44300.96	44349.24	44351.2	44349.45
20	44224.97	44229.24	44225.08	44296.61	44300.75	44296.93	44365.33	44368.93	44365.45			
25	44271.28	44277.52	44271.53	44359.54	44365.64	44360.02						

Table 7: Reported and Calculated Energies for the F(2) component of the NO A-X $v'=0, v''=0$ band

N'	P(2), Wavenumbers			Q(2), Wavenumbers			R(2), Wavenumbers			O(12), Wavenumbers		
	Engleman	Herzberg	Amiot	Engleman	Herzberg	Amiot	Engleman	Herzberg	Amiot	Engleman	Herzberg	Amiot
0										44,074.05	44,074.09	44,074.06
1	44,078.07	44,078.06	44,078.03							44,069.42	44,069.51	44,069.43
2	44,077.40	44,077.46	44,077.38	44,085.95	44,086.01	44,085.98				44,065.31	44,065.48	44,065.34
3	44,077.27	44,077.40	44,077.26	44,089.27	44,089.38	44,089.30	44,097.90	44,097.93	44,097.90	44,061.77	44,062.01	44,061.78
4	44,077.63	44,077.90	44,077.68	44,093.12	44,093.30	44,093.16	44,105.17	44,105.27	44,105.19	44,058.72	44,059.09	44,058.76
5	44,078.59	44,078.96	44,078.63	44,097.51	44,097.77	44,097.54	44,112.98	44,113.16	44,113.02	44,056.23	44,056.73	44,056.28
10	44,091.35	44,092.57	44,091.45	44,127.42	44,128.45	44,127.53	44,160.81	44,160.92	44,160.17		44,053.29	44,052.72
15	44,117.59	44,120.21	44,117.81	44,170.77	44,173.09	44,170.98	44,220.54	44,222.57	44,220.74	44,061.00	44,063.95	44,061.22
20	44,157.44	44,162.10	44,157.85	44,227.71	44,231.87	44,228.04	44,294.47	44,298.28	44,294.84	44,083.85	44,088.96	44,084.26
25	44,211.09	44,218.52	44,211.73	44,298.29	44,305.07	44,298.85		44,388.27	44,382.59	44,120.61	44,128.64	44,121.24

Table 8: Reported and Calculated dEnergies for the F(1) component of the NO A-X $v'=0, v''=0$ band

N'	dP(1), Wavenumbers			dQ(1), Wavenumbers			dR(1), Wavenumbers			dS(21), Wavenumbers		
	Engleman	Herzberg	Amiot	Engleman	Herzberg	Amiot	Engleman	Herzberg	Amiot	Engleman	Herzberg	Amiot
0	44193.94	-0.06	0.01	44198.92	-0.07	-0.03	0.00			0.00		
1	44189.57	-0.09	0.02	44197.83	-0.14	-0.08	44202.94	-0.02	0.02	0.00		
2	44185.82	-0.14	0.03	44197.46	-0.15	-0.03	44205.88	-0.04	0.03	44210.76	-0.15	-0.11
3	44182.66	-0.25	0.00	44197.69	-0.19	-0.02	44209.43	-0.10	0.02	44217.88	0.04	0.10
4	44180.21	-0.30	0.05	44198.50	0.69	-0.05	44213.62	-0.16	0.02	44225.28	-0.14	-0.03
5	44178.32	-0.43	0.03	44199.96	-0.42	-0.07	44218.44	-0.24	0.01	44233.42	-0.22	-0.05
10	44178.32	-1.31	-0.01	44216.67	-1.22	-0.12	44251.92	-0.90	0.01	44283.57	-0.85	-0.10
15	44193.94	-2.58	-0.03	44248.91	-2.50	-0.23	44300.91	-2.05	-0.05	44349.24	-1.96	-0.21
20	44224.97	-4.27	-0.11	44296.61	-4.14	-0.32	44365.33	-3.60	-0.12	0.00		
25	44271.28	-6.24	-0.25	44359.54	-6.10	-0.48	0.00			0.00		

Table 9: Reported and Calculated dEnergies for the F(2) component of the NO A-X v'=0, v''=0 band

N	dP(2), Wavenumbers			dQ(2), Wavenumbers			dR(2), Wavenumbers			dO(12), Wavenumbers		
	Engleman	Herzberg	Amiot	Engleman	Herzberg	Amiot	Engleman	Herzberg	Amiot	Engleman	Herzberg	Amiot
0							0.00			44074.05	-0.04	-0.01
1	44078.07	0.01	0.04							44069.42	-0.09	-0.01
2	44077.40	-0.06	0.02	44085.95	-0.06	-0.03				44065.31	-0.17	-0.03
3	44077.27	-0.13	0.01	44089.27	-0.11	-0.03	44097.90	-0.03	0.00	44061.77	-0.24	-0.01
4	44077.63	-0.27	-0.05	44093.12	-0.18	-0.04	44105.17	-0.10	-0.02	44058.72	-0.37	-0.04
5	44078.59	-0.38	-0.04	44097.51	-0.26	-0.03	44112.98	-0.18	-0.04	44056.23	-0.50	-0.05
10	44091.35	-1.22	-0.10	44127.42	-1.03	-0.11	44160.81	-0.11	0.64			
15	44117.59	-2.62	-0.22	44170.77	-2.32	-0.21	44220.54	-2.03	-0.20	44061.00	-2.95	-0.22
20	44157.44	-4.66	-0.41	44227.71	-4.16	-0.33	44294.47	-3.81	-0.37	44083.85	-5.11	-0.41
25	44211.09	-7.43	-0.64	44298.29	-6.78	-0.56	0.00			44120.61	-8.03	-0.63

Table 10: Reported and Calculated dWavelengths for the F(1) component of the NO A-X v'=0, v''=0 band

N	dP(1), Å			dQ(1), Å			dR(1), Å			dS(21), Å		
	Engleman	Herzberg	Amiot	Engleman	Herzberg	Amiot	Engleman	Herzberg	Amiot	Engleman	Herzberg	Amiot
0	2262.75	0.00323	-0.00036	2262.50	0.00353	0.00148						
1	2262.98	0.00461	-0.00102	2262.55	0.00717	0.00410	2262.29	0.00123	-0.00082			
2	2263.17	0.00702	-0.00169	2262.57	0.00773	0.00159	2262.14	0.00230	-0.00128	2261.89	0.00757	0.00553
3	2263.33	0.01276	-0.00005	2262.56	0.00968	0.00097	2261.96	0.00532	-0.00082	2261.53	-0.00179	-0.00486
4	2263.46	0.01547	-0.00246	2262.52	-0.03537	0.00251	2261.75	0.00818	-0.00102	2261.15	0.00721	0.00158
5	2263.55	0.02224	-0.00133	2262.45	0.02160	0.00369	2261.50	0.01202	-0.00077	2260.73	0.01119	0.00250
10	2263.55	0.06732	0.00072	2261.59	0.06235	0.00609	2259.79	0.04621	-0.00077	2258.17	0.0435	0.00525
15	2262.75	0.13224	0.00169	2259.94	0.12778	0.01185	2257.29	0.10435	0.00245	2254.83	0.0997	0.01073
20	2261.17	0.21835	0.00568	2257.51	0.21117	0.01651	2254.01	0.18283	0.00605			
25	2258.80	0.31848	0.01291	2254.31	0.30985	0.02429						

Table 11: Reported and Calculated dWavelengths for the F(2) component of the NO A-X v'=0, v''=0 band

N	dP(2), Å			dQ(2), Å			dR(2), Å			dO(12), Å		
	Engleman	Herzberg	Amiot	Engleman	Herzberg	Amiot	Engleman	Herzberg	Amiot	Engleman	Herzberg	Amiot
0										2268.91	0.00185	0.00031
1	2268.70	-0.00046	-0.00201							2269.15	0.00484	0.00072
2	2268.74	0.00309	-0.00103	2268.30	0.00288	0.00134				2269.36	0.00865	0.00144
3	2268.74	0.00679	-0.00041	2268.13	0.00561	0.00149	2267.68	0.00154	0.00000	2269.54	0.01241	0.00057
4	2268.72	0.01385	0.00252	2267.93	0.00916	0.00195	2267.31	0.00509	0.00098	2269.70	0.01896	0.00196
5	2268.68	0.01930	0.00232	2267.70	0.01337	0.00154	2266.91	0.00904	0.00185	2269.83	0.02576	0.00258
10	2268.02	0.06275	0.00514	2266.16	0.05315	0.00591	2264.45	0.00574	-0.03272			
15	2266.67	0.13460	0.01130	2263.94	0.11870	0.01056	2361.39	0.10365	0.01007	2269.58	0.15220	0.01159
20	2264.62	0.23902	0.02108	2261.03	0.21265	0.01687	2257.62	0.19427	0.01896	2268.40	0.26307	0.02125
25	2261.88	0.38011	0.03279	2257.42	0.34535	0.02844				2266.51	0.41233	0.03226

How do the deviations between the observed and calculated line positions compare with the resolution of the 2 M vacuum-ultraviolet spectrograph-monochromator? The 2 M vacuum-ultraviolet spectrograph-monochromator wavelength calibration performed on November 29, 1995 provides an absolute wavelength uncertainty of 0.86 Å at a dial reading of 3,425.00 units (2,260.17 Å). This uncertainty is based on the estimated uncertainties of the calculated

coefficients. This uncertainty should introduce only a linear constant offset to the observed emission spectrum and, therefore, not effect the assignments made in our measurements. For these measurements the spectral resolution of the 2 M vacuum-ultraviolet spectrograph-monochromator is $\sim 2 \text{ cm}^{-1}$ which is equivalent to $\sim 0.13 \text{ \AA}$ at $2,597.4 \text{ \AA}$. For $N' \leq 25$ the deviation between the calculated and observed line positions is smaller than the instrumental resolution using the data reported by Amiot *et al.*⁷⁰ for the $\text{NO}(X^2\Pi_r)$ state. The error in the assignments is then limited by the resolution of the 2 M vacuum-ultraviolet spectrograph-monochromator and not the calculated line positions, and the effect on our reported temperatures should be well within the limits of our uncertainties, *i.e.*, $\pm 10\%$.

The next question that arises is, 'How does the use of the Herzberg or Amiot data effect the results that we reported for the rotational temperature of the $\text{NO}(A^2\Sigma^+, v'=0)$ using the term energies and equations reported by Engleman *et al.*⁶⁹?' The reported²¹ rotational temperatures for the product $\text{NO}(A^2\Sigma^+, v'=0)$ observed in the energy transfer reaction $\text{N}_2(A^3\Sigma_u^+, v') + \text{NO}(X^2\Pi_r, v''=0)$ are $(1,272 \pm 49) (1\sigma)$, $(1,349 \pm 18) (1\sigma)$ and $(1,626 \pm 41) \text{ K} (1\sigma)$ at pressures of ~ 2.8 , ~ 2.0 and ~ 1.1 Torr, respectively. To compare the data using the new term energies and energy level equations, the Fractional Areas associated with each emission spectrum were recalculated and the entire data set was recompiled using Quattro Pro v6.0 (Novell). A summary of the calculations is presented in Table 12. The temperatures reported previously were calculated using a sixth order polynomial fit to the Fractional Area Analysis data obtained from an analysis of the synthetically generated $\text{NO}(A^2\Sigma^+, v' \rightarrow X^2\Pi_r, v'')$ γ bands. The results of a similar analysis are presented in the column labeled Engleman 2, $n=6$ in Table 12. As expected, the agreement between the previously reported values²¹ and the re-evaluated data is very good. The small differences are due to the selection of slightly different background intensities for the photoelectric emission spectra. An improvement in the analysis process was made by utilizing a cubic-spline interpolation of the $T_{\text{Rotational}}$ vs $\frac{\text{Area}_{2330-2355}}{\text{Area}_{2330-2372}}$ rather than fitting the data to an

n th-order polynomial. The cubic spline interpolation provides a much smoother fit to the data and a more accurate representation of the data. With the exception of the low pressure data, we

see a slight increase in the estimated rotational temperature of the $\text{NO}(A\ 2\Sigma^+, v'=0)$ using a cubic-spline fit to the data calculated using the Engleman term energies and energy level equations. The estimated rotational temperature of the $\text{NO}(A\ 2\Sigma^+, v'=0)$ is seen to increase slightly when we use the Amiot *et al.*⁷⁰ data for the $\text{NO}(X\ 2\Pi_r)$ state. The Amiot *et al.*⁷⁰ is in very good agreement with that reported previously.

Table 12. Temperature Analysis Summary

	Pressure Torr	Engleman 2, CS	Engleman 2, n = 6	Amiot 2, CS
<Avg> =	2.85	1,317.58	1,297.67	1,322.00
d <Avg> =	0.02	26.50	50.80	27.19
Count =	6.00	6.00	5.00	6.00
<Avg> =	2.16	1,384.18	1,335.33	1,390.38
d <Avg> =	0.01	15.27	12.79	15.64
Count =	42.00	42.00	42.00	42.00
<Avg> =	1.04	1,590.07	1,605.81	1,600.87
d <Avg> =	0.05	49.71	42.79	50.77
Count =	7.00	7.00	6.00	7.00

3.5 GENERAL MODIFICATIONS AND CODE ENHANCEMENTS

In addition to the enhancements made to the code that is used to generate the $\text{NO}(A\ 2\Sigma^+, v' \rightarrow X\ 2\Pi_r, v'')$ γ bands and $\text{NO}(B\ 2\Pi_r, v' \rightarrow X\ 2\Pi_r, v'')$ β bands, synthetic spectra modifications were made to the Data Acquisition Software and Data Analysis Software that is utilized to collect and analyze the experimental data. The data acquisition computer was upgraded from a IBM 286 compatible system to a 386 compatible system.

4 CONCLUSIONS

From these experiments of reacting $\text{NO}(X\ 2\Pi_r, v''=0)$ with $\text{N}_2(A\ 3\Sigma_u^+, v')$ with v' having values of $v'=0$, $v'=0$ and 1, and $v'=0$, 1 and 2 we have obtained branching ratios of emissions associated

with the excited product states. The branching ratio for the $\frac{[\text{NO}(A, v'=0)]}{[\text{NO}(B, v'=0)]} = \frac{\gamma_0}{\beta_0}$ is determined

to be (1.54 ± 0.21) , (3.28 ± 0.42) and (7.67 ± 1.48) for $\text{N}_2(A^3\Sigma_u^+, v')$ vibrational level distributions of $v'=0$, $v'=0$ and 1, and $v'=0$, 1 and 2, respectively. The production efficiency of the $\text{NO}(B^2\Pi_r, v')$ state is much more sensitive to the vibrational level population distribution of the $\text{N}_2(A^3\Sigma_u^+)$ than is the vibrational level distribution of the $\text{NO}(A^2\Sigma^+)$ state. The intensity of the $1, v''$ transition of the $\text{NO}(A^2\Sigma^+, v \rightarrow X^2\Pi_r, v'')$ γ bands is observed to increase by a factor of ~ 2 relative to the intensity of the $0, v''$ transition of the $\text{NO}(A^2\Sigma^+, v' \rightarrow X^2\Pi_r, v'')$ γ bands as the vibrational level population distribution of the $\text{N}_2(A^3\Sigma_u^+, v')$ is shifted from a vibrational level distribution of $1.00 : 0.00 : 0.00$ to $1.00 : 0.29 : 0.11$ for $v'=0$, 1 and 2, respectively. The intensity of the emission from the $0, v''$ transition of the $\text{NO}(B^2\Pi_r, v' \rightarrow X^2\Pi_r, v'')$ b bands is observed to increase by a factor of ~ 5 relative to the intensity of the emission for the $0, v''$ transition of the $\text{NO}(A^2\Sigma^+, v' \rightarrow X^2\Pi_r, v'')$ g bands for the same $\text{N}_2(A^3\Sigma_u^+)$ vibrational level population distributions. It is conceivable, therefore, that a $\text{N}_2(A^3\Sigma_u^+, v')$ distribution which has a greater percentage of its population in $v' \geq 1$ levels compared to our work would result in larger $\frac{[\text{NO}(A, v'=0)]}{[\text{NO}(B, v'=0)]}$ ratios.

Our experimental measurements show that changes in the ratio $\frac{[\text{NO}(A, v'=0)]}{[\text{NO}(B, v'=0)]}$ from the energy

transfer reaction $\text{CO}(a^3\Pi, v') + \text{NO}(X^2\Pi_r)$ are due to changes in the vibrational level population distribution of the $\text{CO}(a^3\Pi)$ state and not due to N_2 impurities in the buffer gases as previously reported¹⁷. As in the case of the energy transfer reaction $\text{N}_2(A^3\Sigma_u^+, v') + \text{NO}(X^2\Pi_r)$, it is necessary to characterize the vibrational level distribution of the metastable precursor state, *e.g.*, the $\text{CO}(a^3\Pi)$ state, when interpreting emission observed using remote sensing techniques. We

see a factor of approximately 6.5 increase in the $[\text{NO}(B^2\Pi_r, v'=0)]$ relative to the $[\text{NO}(A^2\Sigma^+, v'=0)]$ when the vibrational level population distribution of the $\text{CO}(a^3\Pi, v')$ is increased from $[v' \geq 1] \sim 0.016 [v' = 0]$ to $[v' \geq 1] \sim [v' = 0]$. Similar behavior is observed in the energy transfer reaction $\text{N}_2(A^3\Sigma_u^+, v') + \text{NO}(X^2\Pi_r)$ where we⁵⁰ observed a factor of 5 increase in the $[\text{NO}(B^2\Pi_r, v'=0)]$ relative to the $[\text{NO}(A^2\Sigma^+, v'=0)]$ for the $\text{N}_2(A^3\Sigma_u^+)$ vibrational level population distribution of $v' = 0$ and $v' \leq 2$ measurements. To extract the precursor $\text{CO}(a^3\Pi)$ and $\text{N}_2(A^3\Sigma_u^+)$ concentrations from the product emissions from the $\text{NO}(A^2\Sigma^+, v' \rightarrow X^2\Pi_r, v'')$ γ bands and $\text{NO}(B^2\Pi_r, v' \rightarrow X^2\Pi_r, v'')$ β bands, it is necessary to take into account the vibrational level distribution of the precursor states.

The present investigation has answered two questions. First, the $\text{NO}(X^2\Pi_r) + \text{N}(4S, 2D)$ product yield accounts for $\leq 2\%$ of the $\text{N}_2(A^3\Sigma_u^+, v' \leq 2) + \text{O}(3P)$ interaction. This is qualitatively consistent with the high $\text{O}(1S)$ yields observed previously⁷¹⁻⁷³ but somewhat smaller than suggested by those studies. Second, the $\text{NO}(X^2\Pi_r) + \text{NO}(X^2\Pi_r)$ product yield in the reaction $\text{N}_2(A^3\Sigma_u^+, v' \leq 6) + \text{O}_2(X^3\Sigma_g^-, v''=0)$ represents $< 0.1\%$ of the $[\text{N}_2(A^3\Sigma_u^+)]_{\text{Total}}$. The $\text{NO}(X^2\Pi_r) + \text{N}(4S, 2D)$ product yield accounts for $(5.7 \pm 1.1)\%$ of the $\text{N}_2(A^3\Sigma_u^+, v' \leq 6) + \text{O}(3P)$ interaction; however, if we consider the reaction $\text{N}_2(A^3\Sigma_u^+, 3 \leq v' \leq 6) + \text{O}(3P)$ the branching fraction could be as large as $(57 \pm 14)\%$. Our investigation, while ruling out the formation of $\text{NO}(X^2\Pi_r) + \text{N}(4S, 2D)$ from the low vibrational levels of $\text{N}_2(A^3\Sigma_u^+)$, raises the question of a possible v -level dependence for the $\text{NO}(X^2\Pi_r) + \text{N}(4S, 2D)$ product yield in the reaction $\text{N}_2(A^3\Sigma_u^+) + \text{O}(3P)$.

5 REFERENCES

1. M. R. Torr, D. G. Torr, "The role of metastables species in the thermosphere," *Rev. Geophys., Space Phys.* **20**(1), 91 (1982).
2. K. P. Huber, G. Herzberg, Molecular Spectra and Molecular Structure. IV. Constants of Diatomic Molecules, First ed. (Van Nostrand Reinhold Company, New York, 1979), p. 420.
3. L. G. Piper, L. M. Cowles, W. T. Rawlins, "State-to-state excitation of NO(A, $v'=0,1,2$) by N₂(A, $v'=0,1,2$)," *J. Chem. Phys.* **85**, 3369 (1986).
4. D. E. Shemansky, "N₂ Vegard-Kaplan system in absorption," *J. Chem. Phys.* **51**(2), 689 (1969).
5. D. E. Shemansky, N. P. Carleton, "Lifetime of the N₂ Vegard-Kaplan system," *J. Chem. Phys.* **51**, 682 (1969).
6. A. Lofthus, P. H. Krupenie, "The spectrum of molecular nitrogen," *J. Phys. Chem. Ref. Data* **6**(1), 113 (1977).
7. D. C. Cartwright, "Vibrational populations of the excited states of N₂ under auroral conditions," *J. Geophys. Res.* **83**, 517 (1978).
8. M. F. Golde, "REACTIONS OF N₂(A $^3\Sigma_u^+$)," *Int. J. Chem. Kinet.* **20**, 75. (1988).
9. J. W. Dreyer, D. Perner, "Deactivation of N₂(A, $v=0-7$) by ground state nitrogen, ethane, and ethylene measured by kinetic absorption spectroscopy," *J. Chem. Phys.* **58**(3), 1195 (1973).
10. J. W. Dreyer, D. Perner, C. R. Roy, "Rate constants for the quenching of N₂(A, $v=0-8$) by CO, CO₂, NH₃, NO, and O₂," *J. Chem. Phys.* **61**, 3164. (1974).
11. C. R. Roy, J. W. Dreyer, D. Perner, "Rate constants for the quenching of N₂(A, v) by rare gases," *J. Chem. Phys.* **63**, 2131 (1975).
12. K. P. Huber, G. Herzberg, Molecular Spectra and Molecular Structure. IV. Constants of Diatomic Molecules, First ed. (Van Nostrand Reinhold Company, New York, 1979), p. 166.
13. S. G. Tilford, J. D. Simmons, "Atlas of the observed absorption spectrum of Carbon Monoxide between 1060 and 1900 Å," *J. Phys. Chem. Ref. Data* **1**(1), 147 (1972).
14. G. Black, T. G. Slanger, "CO($a^3\Pi$), Its Production, Detection, Deactivation, and Radiative Lifetime," *J. Chem. Phys.* **55**(5), 2164 (1971).
15. T. S. Wauchop, H. P. Broida, "Lifetime and Quenching of Co($a^3\Pi$) Produced by Recombination of Co₂ Ions in a Helium Afterglow," *J. Chem. Phys.* **56**(1), 330 (1972).
16. R. A. Young, G. Van Volkenburgh, "Collisional Deactivation of CO($a^3\Pi$)," *J. Chem. Phys.* **55**(6), 2990 (1971).
17. G. W. Taylor, D. W. Setser, "Quenching rate constants for CO(A $^3\Pi$, $v'=0,1,2$)," *J. Chem. Phys.* **58**(11), 4840 (1973).
18. F. R. Gilmore, Potential Energy Curves for N₂, NO, O₂ and Corresponding Ions (1964).

19. D. L. Albritton, A. L. Schmeltekopf, R. N. Zare, "Potential energy curves for NO⁺," *J. Chem. Phys.* **71**(8), 3271 (1979).
20. J. M. Thomas, F. Kaufman, M. F. Golde, "Rate constants for electronic quenching of N₂(A ³Σ_u⁺, v = 0 -6) BY O₂, NO, CO, N₂O, AND C₂H₄," *J. Chem. Phys.* **86**, 6885 (1987).
21. J. M. Thomas, D. H. Katayama, "Rotational analysis of the nonthermal NO(A ²Σ⁺, v'=0) distribution observed in the N₂(A ³Σ_u⁺, v'=0) + NO(X ²Π, v'=0) energy transfer reaction," *J. Chem. Phys.* **94**(7), 4797 (1991).
22. J. M. Thomas, J. B. Jeffries, F. Kaufman, "Vibrational relaxation of N₂(A ³Σ_u⁺, v=1,2,3) by CH₄ AND CF₄," *Chem. Phys. Lett.* **102**(1), 50 (1983).
23. J. M. Thomas, F. Kaufman, "Rate constants of the reaction of metastable N₂(A ³Σ_u⁺) in v= 0,1,2, and 3 with ground state O₂ and O," *J. Chem. Phys.* **83**(6), 2900 (1985).
24. M. F. Golde, G. H. Ho, W. Tao, J. M. Thomas, "Collisional deactivation of N₂(A, v=0-6) by CH₄, CF₄, H₂, H₂O, CF₃Cl, and CF₂HCl," *J. Phys. Chem.* **93**, 1112 (1989).
25. J. M. Thomas, "Gas phase kinetic studies of metastable molecular nitrogen A state (laser excited fluorescence)," Ph.D. thesis, University Of Pittsburgh, 1986.
26. G. V. Candler, S. Nijhawan, D. Bose, I. D. Boyd, "A Multiple Translational Temperature Gas-Dynamics Model," *Phys. Fluids.* **6**(11), 3776 (1994).
27. D. Bose, G. V. Candler, "Kinetics of the N₂ + O → NO + N Reaction in nonequilibrium flows," *AIAA* **34**, 1 (1996).
28. D. Bose, G. V. Candler, "Thermal Rate Constants of the N₂ + O → NO + N Reaction Using Ab-Initio (3)A" and (3)A' Potential-Energy Surfaces," *J. Chem. Phys.* **104**(8), 2825 (1996).
29. D. Bose, G. V. Candler, "Kinetics of the N₂ + O → NO + N Reaction Under Thermodynamic Nonequilibrium," *Journal of Thermophysics and Heat Transfer* **10**(1), 148 (1996).
30. J. M. Thomas, F. Kaufman, "An Upper Limit on the Formation of NO(X ²Π_r) in the Reactions N₂(A ³Σ_u⁺) + O(3P) and N₂(A ³Σ_u⁺) + O₂(X ³Σ_g⁺) at 298K," *J. Phys. Chem.* **100**(21), 8901 (1996).
31. D. H. Stedman, D. W. Setser, "Chemical applications of metastable argon atoms II. A clean system for the formation of N₂(A)," *Chem. Phys. Lett.* **2**, 542 (1968).
32. D. H. Stedman, D. W. Setser, "Chemical applications of metastable argon atoms. III. Production of krypton and xenon metastable atoms," *J. Chem. Phys.* **52**(8), 3957 (1970).
33. J. M. Thomas, F. Kaufman, "Production and Kinetics of N₂(A ³Σ_u⁺, v'≤3)," XVIth Informal Conference on Photochemistry, Harvard University (20 August, 1984), Abstract (1984).
34. M. J. Mumma, E. C. Zipf, "Calibration of vacuum-ultraviolet monochromators by the molecular branching-ratio technique," *J. Opt. Soc. Am.* **61**, 83 (1971).

35. M. J. Mumma, "Molecular branching-ratio method for intensity calibration of optical systems in the vacuum ultraviolet," *J. Opt. Soc. Am.* **62**, 1459 (1972).
36. H. L. Langhaar, "Steady flow in the transition length of a straight tube," *J. Appl. Mech.* **6**, A55 (1942).
37. J. O. Hirschfelder, C. F. Curtiss, R. B. Bird, Molecular theory of gases and liquids, First ed. (John Wiley & Sons, New York, 1954).
38. T. S. Wauchop, H. P. Broida, "Absolute measurements of light emission from CO_2^+ and CO in the interaction of $\text{He}(2^3\text{S})$ with CO_2^* ," *J. Quant. Spectros. Radiat. Transfer* **12**, 371 (1972).
39. G. W. Taylor, D. W. Setser, "Chemical Applications of Metastable Argon Atoms. Generation, Identification And Characterization of $\text{CO}(a^3\Pi)$," *Chem. Phys. Lett.* **8**, 51. (1971).
40. G. Herzberg, Molecular Spectra and Molecular Structure. I. Spectra of Diatomic Molecules, Second ed. (Van Nostrand Reinhold Company, New York, 1950).
41. R. J. Cvetanovic, D. L. Singleton, G. Paraskevopoulos, "Evaluations of the mean values and standard errors of rate constants and their temperature coefficients," *J. Phys. Chem.* **83**, 50. (1979).
42. R. J. Cvetanovic, R. P. Overend, G. Paraskevopoulos, "Accuracy and precision of gas phase kinetics techniques," *Int. J. Chem. Kinet.* **S1**, 249 (1975).
43. K. P. Huber, G. Herzberg, Molecular Spectra and Molecular Structure. IV. Constants of Diatomic Molecules, First ed. (Van Nostrand Reinhold Company, New York, 1979).
44. J. W. Rabalais, Principles of Ultraviolet Photoelectron Spectroscopy, 1st ed. (John Wiley & Sons, New York, 1977).
45. L. G. Piper, L. M. Cowles, "Einstein coefficients and transition moment variation for the $\text{NO}(A^2\Sigma^+ - X^2\Pi)$ transition," *J. Chem. Phys.* **85**(5), 2419 (1986).
46. L. G. Piper, T. R. Tucker, W. P. Cummings, "Electronic-Transition Moment Variation and Einstein Coefficients for the $\text{NO}(B^2\Pi_r, v' - X^2\Pi_r, v)$ β bands System," *J. Chem. Phys.* **94**(12), 7667 (1991).
47. S. Srinivas, S. V. J. Lakshman, "BASIC program for evaluation of wavenumbers for wavelengths," *American Laboratory* **20**(9), 23 (1988).
48. M. F. Golde, A. M. Moyle, "Study of the products of the reactions of $\text{N}_2(A)$: The effect of vibrational energy in $\text{N}_2(A)$," *Chem. Phys. Lett.* **117**(4), 375 (1985).
49. P. H. Krupenie, The Band Spectrum of Carbon Monoxide, (National Bureau of Standards, Washington, DC, 1966).
50. J. M. Thomas, D. H. Katayama, "Branching fractions of the product $\text{NO}(A^2\Sigma^+, v'=0,1)$ and $\text{NO}(B^2\Pi_r, v'=0)$ emissions observed as a function of v' in the energy transfer reaction $\text{N}_2(A^3\Sigma_u^+, v') + \text{NO}(X^2\Pi_r, v'=0)$," *Chem. Phys. Lett.* **214**(2), 250 (1993).
51. M. P. Iannuzzi, J. B. Jeffries, F. Kaufman, "Product channels of the $\text{N}_2(A) + \text{O}_2$ interaction," *Chem. Phys. Lett.* **87**(6), 570 (1982).

52. E. C. Zipf, "A laboratory study on the formation of nitrous oxide by the reaction of $N_2(A) + O_2 \rightarrow N_2O + O$," *Nature (London)* **287**, 523 (1980).
53. A. R. De Sousa, M. Touzeau, M. Petitdidier, "Quenching reactions of metastable $N_2(A)$ molecules by O_2 ," *Chem. Phys. Lett.* **121**(4,5), 423 (1985).
54. G. Black, R. M. Hill, R. L. Sharpless, T. G. Slinger, N. Albert, "Laboratory studies on N_2O relevant to stratospheric processes," *J. Photochem.* **22**, 369 (1983).
55. M. E. Fraser, L. G. Piper, "Product Branching Ratios from the $N_2(A \ ^3\Sigma_u^+) + O_2$ Interaction," *J. Phys. Chem.* **93**(3), 1107 (1989).
56. I. W. M. Smith, Kinetics and dynamics of elementary gas reactions, ed. (Butterworths, Boston, 1980).
57. N. Sadeghi, D. W. Setser, "Primary $N_2(B)$ vibrational distributions from the excitation-transfer reaction between Kr^* and Xe^* atoms and N_2 ," *Chem. Phys. Lett.* **82**, 44 (1981).
58. J. Balamuta, M. F. Golde, "Quenching of metastable Ar, Kr, and Xe atoms by oxygen-containing compounds: a resonance fluorescence study of reaction products," *J. Chem. Phys.* **76**(5), 2430 (1982).
59. J. Balamuta, M. F. Golde, "Formation of Electronically Excited Oxygen Atoms in the reaction $Ar(^3P_{2,0})$ and $Xe(^3P_{2,0})$ atoms with O_2 ," *J. Phys. Chem.* **86**, 2765 (1982).
60. K. Schofield, "Rate constants for gaseous interactions of $O(2 \ ^1D_2)$ and $O(2 \ ^1S_0)$ - Critical Evaluation," *J. Photochem.* **9**(1), 55 (1978).
61. F. Kaufman, "Reactions of oxygen atoms," *Prog. React. Kinet.* **1**, 1 (1961).
62. T. R. Marrero, E. A. Mason, "Gaseous diffusion coefficients," *J. Phys. Chem. Ref. Data* **1**(1), 3 (1972).
63. D. Levron, A. V. Phelps, "Quenching of $N_2(A)$ by N_2 , Ar, and H_2 ," *J. Chem. Phys.* **69**, 2260 (1978).
64. E. E. Ferguson, F. C. Fehsenfeld, A. L. Schmeltekopf, "Flowing afterglow measurements of ion-neutral reactions," *Adv. At. Mol. Phys.* **5**, 1 (1969).
65. R. P. Fernando, I. W. M. Smith, "Vibrational relaxation of NO by atomic oxygen," *Chem. Phys. Lett.* **66**, 218 (1979).
66. J. C. Stephenson, "Vibrational relaxation of $NO(X \ ^2\Pi, v=1)$ in the temperature range 100-300 K," *J. Chem. Phys.* **60**(11), 4289 (1974).
67. W. B. DeMore, S. P. Sander, D. M. Golden, M. J. Molina, R. F. Hampson, M. J. Kurylo, C. J. Howard, A. R. Ravishankara, "Chemical Kinetics and Photochemical Data for Use in Stratospheric Modeling: Evaluation Number 9," *Jet Propulsion Lab* **90**(1), 1 (1990).
68. H. H. Michels, Correlation diagrams for N_2O in $C_{\infty v}$, C_{2v} and C_s symmetries (1984).
69. R. Engleman Jr., P. E. Rouse, H. M. Peek, V. D. Baiamonte, Beta and gamma band systems of nitric oxide, UC-34 ed. (Federal Scientific and Technical Information (NIST), Springfield, VA, 1969).

70. C. Amiot, R. Bacis, G. Guelachvili, "Infrared study of the $X^2\Pi$ $v=0,1,2$ levels of $^{14}\text{N}^{16}\text{NO}$. Preliminary results on the $v=0, 1$ levels of $^{14}\text{N}^{17}\text{O}$, $^{14}\text{N}^{18}\text{O}$, and $^{15}\text{N}^{16}\text{O}$," *Can. J. Phys.* **56**, 251 (1977).
71. L. G. Piper, "The excitation of $\text{O}(1\text{S})$ in the reaction between $\text{N}_2(\text{A})$ and $\text{O}(3\text{P})$," *J. Chem. Phys.* **77**, 2373 (1982).
72. A. R. De Souza, M. Touzeau, "Quenching reaction of metastable nitrogen molecules $\text{N}_2(\text{A})$ by O and O_2 ," *Int. Conf. Phenom. Ioniz. Gases* **4**, 546 (1983).
73. A. R. De Souza, G. Gousset, M. Touzeau, T. Khiet, "Note on the determination of the efficiency of the reaction $\text{N}_2(\text{A}) + \text{O}(^3\text{P}) \rightarrow \text{N}_2 + \text{O}(1\text{S})$," *J. Phys. B: Atomic Molec. Phys.* **18**, L661 (1985).

6 PRESENTATIONS

- "Energy transfer measurements involving important diatomic molecules: N_2 , NO and CO ," J. M. Thomas and D. H. Katayama, Standard Plume Ultraviolet Radiation Code (SPURC) Technical Direction Meeting, Grumman Corporation, VA, 13-15 April 1993 (Invited talk).
- "Energy transfer measurements involving important diatomic molecules: N_2 , NO and CO ," J. M. Thomas and D. H. Katayama, Standard Plume Ultraviolet Radiation Code (SPURC) Technical Direction Meeting, Grumman Corporation, VA, 12 April 1994 (Invited talk).
- "Rotational temperature of the product $\text{NO}(\text{A } ^2\Sigma^+)$ state formed in the energy transfer reaction $\text{CO}(a^3\Pi, v' \leq 3) + \text{NO}(X^2\Pi_r)$ determined using both high and low resolution detection techniques: a work in progress," Joseph M. Thomas and Daniel H. Katayama, XXII Informal Conference on Photochemistry, University of Minnesota, June 17-21, 1996 (Oral Presentation).

7 PUBLICATIONS

- "Branching fractions of the product $\text{NO}(\text{A } ^2\Sigma^+, v'=0 \text{ and } 1)$ and $\text{NO}(\text{B } ^2\Pi_r, v'=0)$ emissions observed as a function of v' in the energy transfer reaction $\text{N}_2(\text{A } ^3\Sigma_u^+, v') + \text{NO}(X^2\Pi_r, v''=0)$," Joseph M. Thomas and Daniel H. Katayama, *Chem. Phys. Letters* **214**(2), 1993, 250-256.
- "Branching fractions of the product $\text{NO}(\text{A } ^2\Sigma^+, v'=0, 1 \text{ and } 2)$ and $\text{NO}(\text{B } ^2\Pi_r, v'=0)$ emissions observed as a function of v' in the energy transfer reaction $\text{CO}(a^3\Pi, v') + \text{NO}(X^2\Pi_r, v''=0)$," Joseph M. Thomas and Daniel H. Katayama, *Chem. Phys. Letters* **241**, 1995, 583-590.
- "A upper limit on the formation of $\text{NO}(X^2\Pi_r)$ in the reactions $\text{N}_2(\text{A } ^3\Sigma_u^+) + \text{O}(^3\text{P})$ and $\text{N}_2(\text{A } ^3\Sigma_u^+) + \text{O}_2\text{O}_2(X^3\Sigma_g^-)$ at 298 K," Joseph M. Thomas and Frederick Kaufman, *J. Phys. Chem.* **100**(21) (1996) 8901-8906.

“Rotational temperature analysis of the non-thermal $\text{NO}(A\ 2\Sigma^+, v'=0)$ distribution observed in the energy transfer reaction $\text{CO}(a\ 3\Pi, v' \leq 4) + \text{NO}(X\ 2\Pi_r, v''=0)$,” Joseph M. Thomas and Daniel H. Katayama, *to be submitted*.

8 KEYWORD LISTING

Active nitrogen
bimolecular energy transfer
branching fractions
carbon monoxide
 $\text{CO}(a\ 3\Pi)$
emission spectra
energy transfer
kinetics
Metastable nitrogen
 $\text{N}_2(A\ 3\Sigma_u^+)$
nitric oxide

nitrogen monoxide
 $\text{NO}(A\ 2\Sigma^+)$
 $\text{NO}(B\ 2\Pi_r)$
photoelectric emission spectroscopy
plasma chemistry
product emissions
rapidly pumped discharge-flow reactor
rotational temperature
synthetic spectra
vibrational temperature